AIMS Mathematics, 9(9): 24654–23676.
DOI: 10.3934/math.20241201
Received: 20 May 2024
Revised: 15 July 2024
Accepted: 12 August 2024
Published: 22 August 2024

http://www.aimspress.com/journal/Math

Research article

Solving the time fractional q-deformed tanh-Gordon equation: A theoretical analysis using controlled Picard's transform method

Khalid K. Ali[1,*], **Mohamed S. Mohamed**[2], **Weam G. Alharbi**[3] **and M. Maneea**[4]

[1] Mathematics Department, Faculty of Science, Al-Azhar University, Nasr-City, Cairo, Egypt
[2] Department of Mathematics, College of Science, Taif University, P.O. Box 11099, Taif 21944, Saudi Arabia
[3] Department of Mathematics, Faculty of Science, University of Tabuk, Tabuk 71491, Saudi Arabia
[4] Faculty of Engineering, MTI University, Cairo, Egypt

* **Correspondence:** Email: khalidkaram2012@azhar.edu.eg; Tel: +201033530861.

Abstract: This paper presented the formulation and solution of the time fractional q-deformed tanh-Gordon equation, a new extension to the traditional tanh-Gordon equation using fractional calculus, and a q-deformation parameter. This extension aimed to better model physical systems with violated symmetries. The approach taken involved the controlled Picard method combined with the Laplace transform technique and the Caputo fractional derivative to find solutions to this equation. Our results indicated that the method was effective and highlighted our approach in addressing this equation. We explored both the existence and the uniqueness of the solution, and included various 2D and 3D graphs to illustrate how different parameters affect the solution's behavior. This work aimed to contribute to the theoretical framework of mathematical physics and has potential applications across multiple interdisciplinary fields.

Keywords: time-fractional q-deformed tanh-Gordon equation; controlled Picard technique; Laplace transform method; existence; fixed point theorem; fractional calculus
Mathematics Subject Classification: 65Qxx, 97Mxx

1. Introduction

Fractional calculus (FC) and fractional differential equations ($FDEs$) extending beyond integer orders of differentiation and integration, has garnered broad applications across diverse fields [1–3]. In physics, it illuminates anomalous diffusion processes and aids in modeling viscoelastic materials and complex dynamical systems [4, 5]. Engineering exploits FC in signal processing, control theory, and electromagnetics, optimizing system performance and designing efficient filters and antennas [6–8].

Biomedical applications encompass modeling physiological processes such as drug release kinetics, nerve conduction, and bioelectrical impedance analysis [9–11]. Furthermore, FC enhances economic and financial models, refining long-term memory processes in asset price fluctuations and bolstering risk management strategies [12, 13]. Its versatility and applicability continue to inspire innovative solutions across interdisciplinary realms, driving progress in various fields.

The concept of q-deformation, first introduced by Arai, has been integrated into dynamical systems, leading to the breaking of system symmetry. Symmetry breaking occurs when the inherent symmetry of a dynamical system is not evident in its ground or equilibrium state [14]. These q-deformed equations, emerging from the notion of q-deformation which generalizes certain algebraic structures like quantum groups, Lie algebras, and associative algebras, introduce a deformation parameter q that induces significant alterations in their properties compared to classical formulations. They find application in various physical systems in describing the propagation of solitons in optical fibers. Also, it is employed in condensed matter physics to model the dynamics of domain walls in ferromagnetic materials. It also provides a mathematical model for studying nonlinear phenomena in fluid dynamics such as the propagation of waves, the formation of solitons and rogue waves, and the dynamics of vortices and turbulence, as well as having connections to quantum field theory, see [15–17].

H. Eleuch introduced the generalized q-deformed sinh-Gordon equation in 2018, expanding upon the traditional form of the sinh-Gordon equation [18], in the form:

$$\frac{\partial^2 \mathsf{y}}{\partial \varkappa^2} - \frac{\partial^2 \mathsf{y}}{\partial \mathsf{t}^2} = [sinh_q(\mathsf{y}^{\nu})]^{\mathsf{p}} - \varpi, \;\; \mathsf{t} \geq 0, \;\; 0 < q \leq 1, \tag{1.1}$$

where $sinh_q(\mathsf{y})$ is in the form:

$$sinh_q(\mathsf{y}) = \frac{e^{\mathsf{y}} - qe^{-\mathsf{y}}}{2}, \tag{1.2}$$

and ν, p, and ϖ are constants $\in \mathcal{R}$. Subsequently, it has undergone various modifications and treatments either analytically or numerically in several studies [19–21], culminating in its current form:

$$\frac{\partial^2 \mathsf{y}}{\partial \varkappa^2} - \frac{\partial^2 \mathsf{y}}{\partial \mathsf{t}^2} = e^{\epsilon \mathsf{y}}[sinh_q(\mathsf{y}^{\nu})]^{\mathsf{p}} - \varpi, \tag{1.3}$$

and ϵ is constant $\in \mathcal{R}$.

Recently, a new form of q-deformed equations has been introduced in [22] called the q-deformed tanh-Gordon equation. The authors presented an analytical solution using the G'/G method, complemented by a numerical solution employing finite difference techniques. We seek to extend the q-deformed tanh-Gordon equation (*q-deformed TGE*) and express it in fractional format by using the Caputo fractional derivative (CFD) with the goal to find an approximate solution for this equation using the controlled Picard method with Laplace transform and Adomian decomposition. This technique is called controlled Picard transform method ($CPTM$).

The controlled Picard method, in conjunction with Laplace transform (LT) and Adomian decomposition, presents a robust strategy for addressing $FDEs$. This methodology involves a progressive refinement of an initial approximation to approach the exact solution iteratively. Incorporation of the LT enables the conversion of the problem into a set of algebraic equations, simplifying the solving process. Additionally, through Adomian decomposition, $FDEs$ are deconstructed into a series of more manageable differential equations, which are subsequently

solved step by step. This technique boasts numerous merits and exhibits computational efficiency, necessitating fewer iterations compared to alternative numerical methods. However, but it has some limitations, that is, convergence depends on the initial conditions, and this method is typically suitable for initial value problems rather than boundary value problems; for more details, see [23].

The *q-deformed TGE* as presented in [22] is in the form:

$$\frac{\partial^2 \mathsf{y}}{\partial \varkappa^2} - \frac{\partial^2 \mathsf{y}}{\partial \mathsf{t}^2} = \left[tanh_q \mathsf{y}(\varkappa, \mathsf{t})^{\upsilon}\right]^{\mathsf{P}} \left(e^{\epsilon \mathsf{y}(\varkappa,\mathsf{t})} + \zeta q\right)^{\rho} - \varpi, \tag{1.4}$$

where

$$tanh_q(\mathsf{y}) = \frac{e^{\mathsf{y}} - qe^{-\mathsf{y}}}{e^{\mathsf{y}} + qe^{-\mathsf{y}}}, \tag{1.5}$$

and $\upsilon, \epsilon, \mathsf{P}, \varpi, \zeta$, and ρ are constants $\in \mathcal{R}$. As we mentioned before that Eq (1.4) is recently introduced, its solutions are still limited. It has not been addressed or solved in fractional format thus far. Therefore, this study will provide a concise examination of the solutions of the *q-deformed TGE* in fractional form using CFD to show the influence of the q deformed parameter with the fractional derivative parameter.

The time fractional *q-deformed TGE* (TF *q-deformed TGE*) under investigation takes the form:

$${}^{C}\mathfrak{D}_{\mathsf{t}}^{\mathfrak{B}} \mathsf{y}(\varkappa, \mathsf{t}) = \frac{\partial^2 \mathsf{y}}{\partial \varkappa^2} - \left[tanh_q \mathsf{y}(\varkappa, \mathsf{t})^{\upsilon}\right]^{\mathsf{P}} \left(e^{\epsilon \mathsf{y}(\varkappa,\mathsf{t})} + \zeta q\right)^{\rho} - \varpi, \tag{1.6}$$

subject to the initial constraints:

$$\mathsf{y}(\varkappa, 0) = \mathsf{y}_0(\varkappa, \mathsf{t}),$$
$$\mathsf{y}_{\mathsf{t}}(\varkappa, 0) = \mathsf{y}_{0\mathsf{t}}(\varkappa, \mathsf{t}),$$

where ${}^{C}\mathfrak{D}_{\mathsf{t}}^{\mathfrak{B}}$ is the CFD with respect to time, and $\mathfrak{B}$ is the parameter that expresses the order of fractional derivative ($1 < \mathfrak{B} \leq 2$).

This paper is structured as follows: Section 2 presents the basics of CFD, the Adomian polynomials, and a detailed explanation of the steps of $CPTM$. In Section 3, we discuss the existence and uniqueness of the solutions of the proposed equation. In Section 4, we apply the $CPTM$ on the TF *q-deformed TGE* and present the numerical outcomes for the solution. Section 5 clarifies the results in a form of two and three-dimensional graphs to show the influence of the parameters on each other. Finally, Section 6 provides the final remarks of this investigation.

2. Fundamental concepts

2.1. Fractional derivatives

In FC there are various fractional derivatives, including Caputo, Riemann-Liouville, Jumarie, Riesz, Caputo-Fabrizio, Atangana-Baleanu, and others, offering versatile tools for modeling complex phenomena in a form of $FDEs$. Each derivative possesses unique properties and applications tailored to specific problem domains. Focusing on the Caputo fractional derivative, it stands out for its advantageous properties in practical applications. The Caputo derivative incorporates initial conditions naturally, making it well-suited for modeling initial value problems. Furthermore, it exhibits linearity, compatibility with classical calculus, and yields physically meaningful solutions for many physical

systems. Its advantages lie in its ability to handle initial conditions straightforwardly, facilitating the solution process for a wide range of $FDEs$ [24–27].

Definition 2.1. *[2] The Caputo derivative of $\mathfrak{B}$ order is defined by:*

$$ {}^{C}\mathfrak{D}_{\mathsf{z}}^{\mathfrak{B}}\mathcal{F}(\mathsf{z}) = \begin{cases} J^{\ell-\mathfrak{B}}\dfrac{d^{\ell}}{d\mathsf{z}^{\ell}}\mathcal{F}(\mathsf{z}), & \ell-1<\mathfrak{B}<\ell, \\ \\ \dfrac{d^{\ell}}{d\mathsf{z}^{\ell}}\mathcal{F}(\mathsf{z}), & \mathfrak{B}=\ell, \end{cases} \tag{2.1} $$

where $J^{\ell-\mathfrak{B}}$ denotes the Riemann-Liouville fractional integral, which can be expressed as:

$$ J^{\mathfrak{B}}\mathcal{F}(\mathsf{z}) = \frac{1}{\Gamma(\mathfrak{B})}\int_{0}^{\mathsf{z}}(\mathsf{z}-\Upsilon)^{(\mathfrak{B}-1)}\,\mathcal{F}(\Upsilon)\,d\Upsilon, \quad \mathsf{z}>0, \quad \mathfrak{B}\in\mathcal{R}^{+}, \tag{2.2} $$

where, $\mathcal{R}^{+}$ denotes all real positive numbers, and $\Gamma(.)$ denotes the established Gamma function. The operator $J^{\mathfrak{B}}$ satisfies the properties below for $\mathfrak{a},\mathfrak{b}\geq -1$:

$$ J^{\mathfrak{a}}J^{\mathfrak{b}}\mathcal{F}(\mathsf{z}) = J^{\mathfrak{a}+\mathfrak{b}}\mathcal{F}(\mathsf{z}). \tag{2.3} $$

$$ J^{\mathfrak{a}}J^{\mathfrak{b}}\mathcal{F}(\mathsf{z}) = J^{\mathfrak{b}}J^{\mathfrak{a}}\mathcal{F}(\mathsf{z}). \tag{2.4} $$

$$ J^{\mathfrak{a}}\mathsf{z}^{\mathsf{m}} = \frac{\Gamma(\mathsf{m}+1)}{\Gamma(\mathsf{m}+1+\mathfrak{a})}\mathsf{z}^{\mathsf{m}+\mathfrak{a}}. \tag{2.5} $$

CFD satisfies the following properties:

$$ {}^{C}\mathfrak{D}_{\mathsf{z}}^{\mathfrak{B}}\Big[J^{\mathfrak{B}}\mathcal{F}(\mathsf{z})\Big] = \mathcal{F}(\mathsf{z}). \tag{2.6} $$

$$ J^{\mathfrak{B}}\Big[{}^{C}\mathfrak{D}_{\mathsf{z}}^{\mathfrak{B}}\mathcal{F}(\mathsf{z})\Big] = \mathcal{F}(\mathsf{z}) - \sum_{\iota=0}^{\ell-1}\mathcal{F}^{\iota}(0)\frac{\mathsf{z}^{\iota}}{\iota!}, \quad \mathsf{z}>0. \tag{2.7} $$

$$ {}^{C}\mathfrak{D}_{\mathsf{z}}^{\mathfrak{B}}\mathsf{z}^{\mathsf{m}} = \frac{\Gamma(\mathsf{m}+1)}{\Gamma(\mathsf{m}+1-\mathfrak{B})}\mathsf{z}^{\mathsf{m}-\mathfrak{B}}. \tag{2.8} $$

Definition 2.2. *[2, 3] The LT of CFD of order $\mathfrak{B}$ is defined as:*

$$ \mathsf{L}\Big[{}^{C}\mathfrak{D}_{t}^{\mathfrak{B}}\mathcal{F}(\mathsf{z})\Big] = \mathcal{S}^{\mathfrak{B}}\mathsf{L}(\mathcal{F}(\mathsf{z})) - \sum_{\ell=0}^{n-1}\mathcal{S}^{\mathfrak{B}-\ell-1}\mathcal{F}^{(\ell)}(0), \quad n-1<\mathfrak{B}\leq n. \tag{2.9} $$

2.2. Adomian polynomials

The Adomian decomposition method based on establishing the unknown function p in a form of series of decompositions:

$$ \mathsf{p} = \sum_{\ell=0}^{\infty}\mathsf{p}_{\ell}. \tag{2.10} $$

The components p_ℓ calculated iteratively. The nonlinear term $\mathsf{F}(\mathsf{p})$, such as $\mathsf{p}^2, \mathsf{p}^3, sin\mathsf{p}, e^{\mathsf{p}}$, etc. can be represented using Adomian polynomials (*APs*) $\mathscr{A}_\ell$ in the form:

$$F(\mathsf{p}) = \sum_{\ell=0}^{\infty} \mathscr{A}_\ell(\mathsf{p}_0, \mathsf{p}_1, ..., \mathsf{p}_\ell). \tag{2.11}$$

APs find utility in addressing different formats of nonlinearity. Originally proposed by Adomian (see [28]) a methodology for computing these polynomials was subsequently corroborated through formal validations. Further approaches have emerged, encompassing methodologies rooted in Taylor series and analogous techniques, as elucidated in references [29–31].

The calculation of *APs*, denoted as $\mathscr{A}_\mathsf{r}$, for the nonlinear component $F(\mathsf{p})$, can be achieved utilizing the general formula:

$$\mathscr{A}_\mathsf{r} = \frac{1}{\mathsf{r}!}\frac{\mathsf{d}^\mathsf{r}}{\mathsf{d}v^\mathsf{r}}\Big[F\Big(\sum_{\ell=0}^{\mathsf{r}} v^\ell \mathsf{p}_\ell\Big)\Big]_{v=0}, \qquad \mathsf{r} = 0, 1, 2, ... \tag{2.12}$$

Equation (2.12) can be expanded as:

$$\begin{aligned}
&\mathscr{A}_0 = F(\mathsf{p}_0),\\
&\mathscr{A}_1 = \mathsf{p}_1 F'(\mathsf{p}_0),\\
&\mathscr{A}_2 = \mathsf{p}_2 F'(\mathsf{p}_0) + \frac{1}{2!}\mathsf{p}_1^2 F''(\mathsf{p}_0),\\
&\mathscr{A}_3 = \mathsf{p}_3 F'(\mathsf{p}_0) + \mathsf{p}_1\,\mathsf{p}_2 F''(\mathsf{p}_0) + \frac{1}{3!}\mathsf{p}_1^3 F'''(\mathsf{p}_0).\\
&\vdots
\end{aligned} \tag{2.13}$$

From Eq (2.13), we notice that $\mathscr{A}_0$ relies only on p_0, $\mathscr{A}_1$ relies only on p_0 and p_1, $\mathscr{A}_2$ relies only on p_0–p_2, etc.

2.3. Controlled Picard transform method

The Picard method was first initiated by Émile Picard in 1890, and it has been modified several times. One crucial modification involves the incorporation of a small parameter indicated by $\hbar$, which regulates the convergence rate and accuracy of the iterative process and also by utilizing the *LT* that enables the transformation of the differential equation into an algebraic equation, simplifying the solution process, [23, 32, 33]. In this study, we merge the controlled Picard method with *LT* and *AP* to be able to deal with the nonlinear terms; this is because the *APs* facilitate the decomposition of nonlinear terms, enabling systematic approximation of the solution.

The following steps summarize how to apply the *CPTM* to a nonlinear *FDE*. Assume the general form of the fractional partial differential equation (*FPDE*):

$${}^{C}\mathfrak{D}_\mathsf{t}^{\mathfrak{B}}\mathsf{y}(\varkappa, \mathsf{t}) + \mathscr{L}\{\mathsf{y}(\varkappa, \mathsf{t})\} + \mathscr{N}\{\mathsf{y}(\varkappa, \mathsf{t})\} = \Xi(\varkappa, \mathsf{t}), \quad \mathsf{t} > 0, \quad 1 < \mathfrak{B} \leqslant 2, \tag{2.14}$$

related to the initial constraints:

$$\begin{aligned}
&\mathsf{y}(\varkappa, 0) = \mathsf{y}_0,\\
&\mathsf{y}_\mathsf{t}(\varkappa, 0) = \frac{\partial \mathsf{y}(\varkappa, 0)}{\partial \mathsf{t}} = \mathsf{y}_{0\mathsf{t}},
\end{aligned}$$

where, $\mathscr{L}\{y(\varkappa,\mathsf{t})\}$ and $\mathscr{N}\{y(\varkappa,\mathsf{t})\}$ indicate the linear and nonlinear terms in the equation, while $\Xi(\varkappa,\mathsf{t})$ indicates the source term.

Apply *LT* to both sides of Eq (2.14),

$$\mathsf{L}\Big[{}^{C}\mathfrak{D}_{\mathsf{t}}^{\mathfrak{B}}\mathsf{y}(\varkappa,\mathsf{t})\Big]+\mathsf{L}\Big[\mathscr{L}\{\mathsf{y}(\varkappa,\mathsf{t})\}+\mathscr{N}\{\mathsf{y}(\varkappa,\mathsf{t})\}\Big]=\mathsf{L}\Big[\Xi(\varkappa,\mathsf{t})\Big]. \tag{2.15}$$

By using definition 2.2 of *LP* (2.15) becomes,

$$\mathcal{S}^{\mathfrak{B}}\mathsf{L}\{\mathsf{y}(\varkappa,\mathsf{t})\}-\sum_{\ell=0}^{n-1}\mathcal{S}^{\mathfrak{B}-\ell-1}\mathsf{y}^{(\ell)}(\varkappa,0)=-\mathsf{L}\Big[\mathscr{L}\{\mathsf{y}(\varkappa,\mathsf{t})\}+\mathscr{N}\{\mathsf{y}(\varkappa,\mathsf{t})\}\Big]+\mathsf{L}\Big[\Xi(\varkappa,\mathsf{t})\Big]. \tag{2.16}$$

For $1<\mathfrak{B}\leqslant 2$,

$$\mathsf{Y}(\varkappa,\mathcal{S})=\frac{1}{\mathcal{S}}\mathsf{y}(\varkappa,0)-\frac{1}{\mathcal{S}^{2}}\mathsf{y}_{\mathsf{t}}(\varkappa,0)-\frac{1}{\mathcal{S}^{\mathfrak{B}}}\mathsf{L}\Big[\mathscr{L}\{\mathsf{y}(\varkappa,\mathsf{t})\}+\mathscr{N}\{\mathsf{y}(\varkappa,\mathsf{t})\}\Big]+\frac{1}{\mathcal{S}^{\mathfrak{B}}}\mathsf{L}\Big[\Xi(\varkappa,\mathsf{t})\Big]. \tag{2.17}$$

Apply the inverse Laplace on the Eq (2.17),

$$\mathsf{y}(\varkappa,\mathsf{t})=\mathsf{L}^{-1}\Big\{\frac{1}{\mathcal{S}}\mathsf{y}(\varkappa,0)-\frac{1}{\mathcal{S}^{2}}\mathsf{y}_{\mathsf{t}}(\varkappa,0)-\frac{1}{\mathcal{S}^{\mathfrak{B}}}\mathsf{L}\Big[\mathscr{L}\{\mathsf{y}(\varkappa,\mathsf{t})\}+\mathscr{N}\{\mathsf{y}(\varkappa,\mathsf{t})\}\Big]+\frac{1}{\mathcal{S}^{\mathfrak{B}}}\mathsf{L}\Big[\Xi(\varkappa,\mathsf{t})\Big]\Big\}, \tag{2.18}$$

hence, the recurrence relation of Picard becomes:

$$\mathsf{y}_{\ell+1}(\varkappa,\mathsf{t})=\mathsf{y}(\varkappa,0)+\mathsf{t}\mathsf{y}_{\mathsf{t}}(\varkappa,0)-\mathsf{L}^{-1}\Big\{\frac{1}{\mathcal{S}^{\mathfrak{B}}}\mathsf{L}\Big[\mathscr{L}\{\mathsf{y}_{\ell}(\varkappa,\mathsf{t})\}+\mathscr{N}\{\mathsf{y}_{\ell}(\varkappa,\mathsf{t})\}-\Xi(\varkappa,\mathsf{t})\Big]\Big\}. \tag{2.19}$$

To merge the parameter $\hbar$ into the recurrence relation of Picard formula (2.19), we write Eq (2.14) as:

$$\Theta\Big(\varkappa,\mathsf{t},\mathsf{y}(\varkappa,\mathsf{t}),\mathfrak{B}\Big)+\mathscr{L}\{\mathsf{y}(\varkappa,\mathsf{t})\}+\mathscr{N}\{\mathsf{y}(\varkappa,\mathsf{t})\}-\Xi(\varkappa,\mathsf{t})=0, \tag{2.20}$$

or

$$\Theta\Big(\varkappa,\mathsf{t},\mathsf{y}(\varkappa,\mathsf{t}),\mathfrak{B}\Big)=0, \tag{2.21}$$

hence,

$$\hbar\,\Theta\Big(\varkappa,\mathsf{t},\mathsf{y}(\varkappa,\mathsf{t}),\mathfrak{B}\Big)=0. \tag{2.22}$$

Add and subtract ${}^{C}\mathfrak{D}_{\mathsf{t}}^{\mathfrak{B}}\mathsf{y}(\varkappa,\mathsf{t})$ to the left-hand side of Eq (2.22):

$${}^{C}\mathfrak{D}_{\mathsf{t}}^{\mathfrak{B}}\mathsf{y}(\varkappa,\mathsf{t})+\hbar\,\Theta\Big(\varkappa,\mathsf{t},\mathsf{y}(\varkappa,\mathsf{t}),\mathfrak{B}\Big)-{}^{C}\mathfrak{D}_{\mathsf{t}}^{\mathfrak{B}}\mathsf{y}(\varkappa,\mathsf{t})=0. \tag{2.23}$$

Let

$$\Theta^{*}\Big(\varkappa,\mathsf{t},\mathsf{y}(\varkappa,\mathsf{t}),\mathfrak{B},\hbar\Big)=-{}^{C}\mathfrak{D}_{\mathsf{t}}^{\mathfrak{B}}\mathsf{y}(\varkappa,\mathsf{t})+\hbar\,\Theta\Big(\varkappa,\mathsf{t},\mathsf{y}(\varkappa,\mathsf{t}),\mathfrak{B}\Big). \tag{2.24}$$

Therefore, Eq (2.23) can be written in the form:

$${}^{C}\mathfrak{D}_{\mathsf{t}}^{\mathfrak{B}}\mathsf{y}(\varkappa,\mathsf{t})+\Theta^{*}\Big(\varkappa,\mathsf{t},\mathsf{y}(\varkappa,\mathsf{t}),\mathfrak{B},\hbar\Big)=0. \tag{2.25}$$

By applying the recurrence formula (2.19) into the relation presented in Eq (2.25), we obtain:

$$\mathsf{y}_{\ell+1}(\varkappa,\mathsf{t}) = \mathsf{y}(\varkappa,0) + \mathsf{t}\mathsf{y}_{\mathsf{t}}(\varkappa,0) - \mathsf{L}^{-1}\Big\{\frac{1}{\mathcal{S}^{\mathfrak{B}}}\mathsf{L}\Big[\hbar[{}^{C}\mathfrak{D}_{\mathsf{t}}^{\mathfrak{B}}\mathsf{y}(\varkappa,\mathsf{t}) + \Theta(\varkappa,\mathsf{t},\mathsf{y}(\varkappa,\mathsf{t}),\mathfrak{B})]\Big]\Big\}. \tag{2.26}$$

The final recurrence relation of Picard takes the form:

$$\mathsf{y}_{\ell+1}(\varkappa,\mathsf{t}) = \hbar\mathsf{y}_0(\varkappa,\mathsf{t}) + (1-\hbar)\mathsf{y}_{\ell} - \hbar\mathsf{L}^{-1}\Big\{\frac{1}{\mathcal{S}^{\mathfrak{B}}}\mathsf{L}\Big[\mathscr{L}\{\mathsf{y}_{\ell}(\varkappa,\mathsf{t})\} + \mathscr{N}\{\mathsf{y}_{\ell}(\varkappa,\mathsf{t})\} - \Xi(\varkappa,\mathsf{t})\Big]\Big\}, \tag{2.27}$$

where $\mathsf{y}_0(\varkappa,\mathsf{t}) = \mathsf{y}(\varkappa,0) + \mathsf{t}\mathsf{y}_{\mathsf{t}}(\varkappa,0)$, and $\ell = 0, 1, 2, ...$

To determine the values of $\hbar$ that lead to faster convergence, we plot the relationship between the obtained solution and $\hbar$, called the $\hbar$-curves. The region where the solution converges rapidly corresponds to the part of the curve parallel to the x-axis.

3. The existence and the uniqueness analysis

In this section, we will conduct a theoretical investigation into the *TF q-deformed TGE*, encompassing examinations of its existence and uniqueness. Equation (1.6) can be written in a general form as:

$${}^{C}\mathfrak{D}_{\mathsf{t}}^{\mathfrak{B}}\mathsf{y}(\varkappa,\mathsf{t}) = F(\mathsf{y},\mathsf{y}_{\varkappa\varkappa}), \quad 1 < \mathfrak{B} \leq 2, \tag{3.1}$$

with starting constraints:

$$\mathsf{y}(\varkappa,0) = h(\varkappa),$$
$$\mathsf{y}_{\mathsf{t}}(\varkappa,0) = k(\varkappa).$$

First, let us consider the following important definitions and theorems:

Definition 3.1. *Assume there exists a normed space represented by* $(\mathsf{y}, \| \ . \ \|)$. *A contraction on* y *denotes a mapping* $\mathsf{M} : \mathsf{y} \longrightarrow \mathsf{y}$ *satisfying the condition* $\mathsf{y}_1, \mathsf{y}_2 \in \mathsf{y}$.

$$\| \mathsf{M}(\mathsf{y}_1) - \mathsf{M}(\mathsf{y}_2) \| \leq \varepsilon \| \mathsf{y}_1 - \mathsf{y}_2 \|,$$

where ε *is a real value* $\in [0, 1]$.

Theorem 3.2. *[34] (Banach fixed point theorem) Each contraction mapping within a complete metric space possesses a unique fixed point.*

Theorem 3.3. *[35] (Schaefer-Krasnoselskii fixed point theorem) Suppose* Y *represents a convex subset of a closed and bounded Banach space* $\mathcal{X}$, *and let* $\mathsf{M} : \mathsf{Y} \longrightarrow \mathsf{Y}$ *be a mapping that is completely continuous. In such a case,* M *necessarily possesses a fixed point within* M.

Definition 3.4. *Consider* $C(\Omega, \mathcal{R})$ *is a Banach space of all continuous functions from* Ω *to* $\mathcal{R}$ *with* $\| \ . \ \|_{\infty}$ *where* $\| \mathsf{y} \|_{\infty} = \sup\{|\mathsf{y}|, (\varkappa,\mathsf{t}) \in \Omega\}$.

According to Eq (3.1), suppose that the following propositions are hold:

$\mathbb{P}_1$: There is a constant δ such that:

$$|\mathsf{y}_{1\varkappa\varkappa} - \mathsf{y}_{2\varkappa\varkappa}| \leq \delta|\mathsf{y}_1 - \mathsf{y}_2|,$$

which is valid for all $(\varkappa, \mathsf{t}) \in \Omega$ and $\mathsf{y} \in C(\Omega, \mathcal{R})$.

$\mathbb{P}_2$: There are constants ϱ_1 and ϱ_2 such that:

$$|F(\mathsf{y}_1, \mathsf{y}_{1\varkappa\varkappa}) - F(\mathsf{y}_2, \mathsf{y}_{2\varkappa\varkappa})| \leq \varrho_1|\mathsf{y}_1 - \mathsf{y}_2| + \varrho_2|\mathsf{y}_{1\varkappa\varkappa} - \mathsf{y}_{2\varkappa\varkappa}|,$$

which is valid for all $(\varkappa, \mathsf{t}) \in \Omega$ and $\mathsf{y} \in C(\Omega, \mathcal{R})$.

Theorem 3.5. *If the above propositions hold; and if* $\dfrac{\mathsf{t}^{\mathfrak{B}}}{\Gamma(\mathfrak{B}+1)}(\varrho_1 + \delta\varrho_2) < 1$, *then, the problem described in Eq* (3.1) *possesses a unique solution.*

Proof. We aim to convert the problem stated in Eq (3.1) into a fixed-point problem. For the operator:

$$\Lambda : C(\Omega, \mathcal{R}) \to C(\Omega, \mathcal{R}),$$

$$\Lambda(\mathsf{y}(\varkappa, \mathsf{t})) = h(\varkappa) + \mathsf{t}\,k(\varkappa) + J_{\mathsf{t}}^{\mathfrak{B}}\Big(F(\mathsf{y}, \mathsf{y}_{\varkappa\varkappa})\Big), \quad 1 < \mathfrak{B} \leq 2.$$

Clearly, the operator Λ constitutes the solution to the problem. Now, we apply the Banach fixed-point theorem to demonstrate that the operator Λ possesses a fixed point. Let $\mathsf{y}_1,\ \mathsf{y}_1 \in C(\Omega, \mathcal{R})$, then for every $(\varkappa, \mathsf{t}) \in \Omega$:

$$\begin{aligned}
|\Lambda\mathsf{y}_1(\varkappa, \mathsf{t}) - \Lambda\mathsf{y}_2(\varkappa, \mathsf{t})| &= J_{\mathsf{t}}^{\mathfrak{B}}\Big|F(\mathsf{y}_1, \mathsf{y}_{1\varkappa\varkappa}) - F(\mathsf{y}_2, \mathsf{y}_{2\varkappa\varkappa})\Big| \\
&\leq J_{\mathsf{t}}^{\mathfrak{B}}\Big(\varrho_1|\mathsf{y}_1 - \mathsf{y}_2| + \varrho_2|\mathsf{y}_{1\varkappa\varkappa} - \mathsf{y}_{2\varkappa\varkappa}|\Big) \\
&\leq J_{\mathsf{t}}^{\mathfrak{B}}\Big(\varrho_1|\mathsf{y}_1 - \mathsf{y}_2| + \varrho_2\delta|\mathsf{y}_1 - \mathsf{y}_2|\Big),
\end{aligned}$$

therefore,

$$\begin{aligned}
|\Lambda\mathsf{y}_1(\varkappa, \mathsf{t}) - \Lambda\mathsf{y}_2(\varkappa, \mathsf{t})| &\leq \frac{\mathsf{t}^{\mathfrak{B}}}{\Gamma(\mathfrak{B}+1)}\Big(\varrho_1 + \varrho_2\delta\Big)\Big|\mathsf{y}_1 - \mathsf{y}_2\Big| \\
&\leq \frac{\mathsf{t}^{\mathfrak{B}}}{\Gamma(\mathfrak{B}+1)}\Big(\varrho_1 + \varrho_2\delta\Big)\sup\Big|\mathsf{y}_1 - \mathsf{y}_2\Big| \\
&\leq \frac{\mathsf{t}^{\mathfrak{B}}}{\Gamma(\mathfrak{B}+1)}\Big(\varrho_1 + \varrho_2\delta\Big)\Big\|\mathsf{y}_1 - \mathsf{y}_2\Big\|_{\infty}.
\end{aligned}$$

Thus, according to the relation $\dfrac{\mathsf{t}^{\mathfrak{B}}}{\Gamma(\mathfrak{B}+1)}(\varrho_1 + \delta\varrho_2) < 1$, the operator Λ is identified as a contraction. As an immediate result of the Banach fixed-point theorem, it follows that Λ possesses a unique fixed point, which concludes the theorem's proof. □

Next, we establish the conditions that guarantees the existence of the solution utilizing Schaefer's fixed-point theorem.

Theorem 3.6. *If the following conditions are met, then, the equation presented in* (3.1) *possesses at least one solution within* $C(\Omega, \mathcal{R})$*:*

Suppose that $\mathsf{y} : \Omega \to \mathcal{R}$ *is continuous, and,*

Condition 1. *There is a constant* $\omega > 0$ *in which*

$$|F(\mathsf{y}, \mathsf{y}_{\varkappa\varkappa})| \leq \omega, \quad for\, each\, (\varkappa, \mathsf{t}) \in \Omega \text{ and } \mathsf{y} \in C(\Omega, \mathcal{R}).$$

Condition 2. *There are two constants* $\eta_1, \eta_2 > 0$ *in which*

$$|F(\mathsf{y}(\varkappa_1, \mathsf{t}_1), \mathsf{y}_{\varkappa\varkappa}(\varkappa_1, \mathsf{t}_1)) - F(\mathsf{y}(\varkappa_2, \mathsf{t}_2), \mathsf{y}_{\varkappa\varkappa}(\varkappa_2, \mathsf{t}_2))| \leq \eta_1 |\mathsf{y}(\varkappa_1, \mathsf{t}_1) - \mathsf{y}(\varkappa_2, \mathsf{t}_2)| + \eta_2 |\mathsf{y}_{\varkappa_1\varkappa_1}(\varkappa_1, \mathsf{t}_1) - \mathsf{y}_{\varkappa_2\varkappa_2}(\varkappa_2, \mathsf{t}_2)|,$$

where $(\varkappa_1, \mathsf{t}_1)$ *and* $(\varkappa_2, \mathsf{t}_2) \in \Omega$, *and* $\mathsf{y} \in C(\Omega, \mathcal{R})$.

Condition 3. *There is a constant* $\wp > 0$ *in which*

$$|\mathsf{y}_{\varkappa_1\varkappa_1}(\varkappa_1, \mathsf{t}_1) - \mathsf{y}_{\varkappa_2\varkappa_2}(\varkappa_2, \mathsf{t}_2)| \leq \wp |\mathsf{y}(\varkappa_1, \mathsf{t}_1) - \mathsf{y}(\varkappa_2, \mathsf{t}_2)|,$$

for each $(\varkappa_1, \mathsf{t}_1)$ *and* $(\varkappa_2, \mathsf{t}_2) \in \Omega$, *and* $\mathsf{y} \in C(\Omega, \mathcal{R})$.

Condition 4. *There are two constants* $\ell_1,\ \ell_2 > 0$ *in which:*

$$|\mathsf{y}(\varkappa_1, \mathsf{t}_1) - \mathsf{y}(\varkappa_2, \mathsf{t}_2)| \leq \ell_1 |\varkappa_1 - \varkappa_2| + \ell_2 |\mathsf{t}_1 - \mathsf{t}_2|.$$

Proof. Suppose y_m is a sequence converging to y in $C(\Omega, \mathcal{R})$, then, for each $(\varkappa, \mathsf{t})$ Ω, it holds that:

$$|\Lambda \mathsf{y}_m(\varkappa, \mathsf{t}) - \Lambda \mathsf{y}(\varkappa, \mathsf{t})| = J_{\mathsf{t}}^{\mathfrak{B}} \left| F(\mathsf{y}_m, \mathsf{y}_{m\varkappa\varkappa}) - F(\mathsf{y}, \mathsf{y}_{\varkappa\varkappa}) \right|.$$

By utilizing the relation $\dfrac{\mathsf{t}^{\mathfrak{B}}}{\Gamma(\mathfrak{B}+1)}(\varrho_1 + \delta\varrho_2) < 1$, we have

$$|\Lambda \mathsf{y}_m(\varkappa, \mathsf{t}) - \Lambda \mathsf{y}(\varkappa, \mathsf{t})| \leq \frac{\mathsf{t}^{\mathfrak{B}}}{\Gamma(\mathfrak{B}+1)}(\varrho_1 + \delta\varrho_2) \|\mathsf{y}_m - \mathsf{y}\|_\infty.$$

Since y is continuous, it follows that $\|\Lambda \mathsf{y}_m(\varkappa, \mathsf{t}) - \Lambda \mathsf{y}(\varkappa, \mathsf{t})\|_\infty$ tends to *zero* as m tends to ∞.

Now, we want to prove that, the mapping Λ maps bounded sets into bounded sets:

$$\begin{aligned} |\Lambda \mathsf{y}(\varkappa, \mathsf{t})| &= \left| h(\varkappa) + \mathsf{t}\, k(\varkappa) + J_{\mathsf{t}}^{\mathfrak{B}} \Big(F(\mathsf{y}, \mathsf{y}_{\varkappa\varkappa}) \Big) \right| \\ &\leq |h(\varkappa)| + |\mathsf{t}\, k(\varkappa)| + J_{\mathsf{t}}^{\mathfrak{B}}(\nu) \\ &\leq |h(\varkappa)| + |\mathsf{t}\, k(\varkappa)| + \frac{\mathsf{t}^{\mathfrak{B}}}{\Gamma(\mathfrak{B}+1)}\omega. \end{aligned}$$

Hence, $\|\Lambda \mathsf{y}(\varkappa, \mathsf{t})\|_\infty \leq |h(\varkappa)| + |\mathsf{t}\, k(\varkappa)| + \dfrac{\mathsf{t}^{\mathfrak{B}}}{\Gamma(\mathfrak{B}+1)}\omega$, which means $\|\Lambda \mathsf{y}(\varkappa, \mathsf{t})\|_\infty < \infty$. Next, we want to show that, the mapping Λ is equi-continuous on $C(\Omega, \mathcal{R})$. To do that, let $(\varkappa_1, \mathsf{t}_1)$, $(\varkappa_2, \mathsf{t}_2) \in \Omega$ and

$\varkappa_1 < \varkappa_2,\ \mathsf{t}_1 < \mathsf{t}_2$, then:

$$\begin{aligned}
|\Lambda \mathsf{y}(\varkappa_1, \mathsf{t}_1) - \Lambda \mathsf{y}(\varkappa_2, \mathsf{t}_2)| &= J_{\mathsf{t}}^{\mathfrak{B}} \left| F(\mathsf{y}(\varkappa_1, \mathsf{t}_1), \mathsf{y}_{\varkappa_1\varkappa_1}(\varkappa_1, \mathsf{t}_1)) - F(\mathsf{y}(\varkappa_2, \mathsf{t}_2), \mathsf{y}_{\varkappa_2\varkappa_2}(\varkappa_2, \mathsf{t}_2)) \right| \\
&\leq J_{\mathsf{t}}^{\mathfrak{B}} \Big(\eta_1 |\mathsf{y}(\varkappa_1, \mathsf{t}_1) - \mathsf{y}(\varkappa_2, \mathsf{t}_2)| + \eta_2 |\mathsf{y}_{\varkappa_1\varkappa_1}(\varkappa_1, \mathsf{t}_1) - \mathsf{y}_{\varkappa_2\varkappa_2}(\varkappa_2, \mathsf{t}_2)| \Big) \\
&\leq J_{\mathsf{t}}^{\mathfrak{B}} \Big(\eta_1 |\mathsf{y}(\varkappa_1, \mathsf{t}_1) - \mathsf{y}(\varkappa_2, \mathsf{t}_2)| + \eta_2 \wp |\mathsf{y}(\varkappa_1, \mathsf{t}_1) - \mathsf{y}(\varkappa_2, \mathsf{t}_2)| \Big) \\
&\leq \frac{\mathsf{t}^{\mathfrak{B}}}{\Gamma(\mathfrak{B}+1)} \Big((\eta_1 + \eta_2 \wp)(\ell_1 |\varkappa_1 - \varkappa_2| + \ell_2 |\mathsf{t}_1 - \mathsf{t}_2|) \Big) \\
&\leq \frac{\mathsf{t}^{\mathfrak{B}}}{\Gamma(\mathfrak{B}+1)} \Big((\eta_1 + \eta_2 \wp)(\ell_1 \parallel \varkappa_1 - \varkappa_2 \parallel_\infty + \ell_2 \parallel \mathsf{t}_1 - \mathsf{t}_2 \parallel_\infty) \Big).
\end{aligned}$$

Finally,

$$|\Lambda \mathsf{y}(\varkappa_1, \mathsf{t}_1) - \Lambda \mathsf{y}(\varkappa_2, \mathsf{t}_2)| \leq \frac{\mathsf{t}^{\mathfrak{B}}}{\Gamma(\mathfrak{B}+1)} \Big((\eta_1 + \eta_2 \wp)(\ell_1 \parallel \varkappa_1 - \varkappa_2 \parallel_\infty + \ell_2 \parallel \mathsf{t}_1 - \mathsf{t}_2 \parallel_\infty) \Big). \tag{3.2}$$

The right-hand side of the inequality (3.2) tends to *zero* as $\varkappa_1 \longrightarrow \varkappa_2$ and $\mathsf{t}_1 \longrightarrow \mathsf{t}_2$ and it is independent of y, which implies that the mapping $\Lambda : (\Omega, \mathcal{R}) \longrightarrow C(\Omega, \mathcal{R})$ is continuous and completely continuous. As a result of Schaefer's fixed point theorem, we conclude that operator Λ possesses a fixed point, serving as a solution to the problem outlined in Eq (3.1). □

4. Implementation of $CPTM$ on the TF *q-deformed* TGE

Recall Eq (1.6) once again:

$$^{C}\mathfrak{D}_{\mathsf{t}}^{\mathfrak{B}} \mathsf{y}(\varkappa, \mathsf{t}) = \frac{\partial^2 \mathsf{y}}{\partial \varkappa^2} - \Big[tanh_q \mathsf{y}(\varkappa, \mathsf{t})^{\upsilon} \Big]^{\mathsf{P}} \Big(e^{\epsilon \mathsf{y}(\varkappa, \mathsf{t})} + \zeta q \Big)^{\rho} - \varpi. \tag{4.1}$$

According to the values of the constants $\upsilon, \mathsf{P}, \epsilon, \zeta, \rho$, and ϖ, we will investigate Eq (4.1) in two cases:
Case I. For $\epsilon = 2$, $\upsilon = \mathsf{P} = \zeta = \rho = 1$, and $\varpi = -q$.

Using the relations (1.5) and (4.1) can be simplified into the form:

$$^{C}\mathfrak{D}_{\mathsf{t}}^{\mathfrak{B}} \mathsf{y} = \mathsf{y}_{\varkappa\varkappa} - e^{2\mathsf{y}}, \qquad 1 < \mathfrak{B} \leq 2, \tag{4.2}$$

related to the constraints:

$$
\begin{aligned}
\mathsf{y}(\varkappa,0) &= \frac{1}{2}ln\Bigg[\mathscr{R}_0+\mathscr{R}_1\left(\frac{\sqrt{\mathcal{E}^2-4\nu}\left(\mathsf{P}_2\cos\left(\frac{1}{2}(\mathsf{k}\varkappa)\sqrt{\mathcal{E}^2-4\nu}\right)-\mathsf{P}_1\sin\left(\frac{1}{2}(\mathsf{k}\varkappa)\sqrt{\mathcal{E}^2-4\nu}\right)\right)}{2\left(\mathsf{P}_1\cos\left(\frac{1}{2}(\mathsf{k}\varkappa)\sqrt{\mathcal{E}^2-4\nu}\right)+\mathsf{P}_2\sin\left(\frac{1}{2}(\mathsf{k}\varkappa)\sqrt{\mathcal{E}^2-4\nu}\right)\right)}-\frac{\mathcal{E}}{2}\right)\\
&\quad+\mathscr{R}_2\left(\frac{\sqrt{\mathcal{E}^2-4\nu}\left(\mathsf{P}_2\cos\left(\frac{1}{2}(\mathsf{k}\varkappa)\sqrt{\mathcal{E}^2-4\nu}\right)-\mathsf{P}_1\sin\left(\frac{1}{2}(\mathsf{k}\varkappa)\sqrt{\mathcal{E}^2-4\nu}\right)\right)}{2\left(\mathsf{P}_1\cos\left(\frac{1}{2}(\mathsf{k}\varkappa)\sqrt{\mathcal{E}^2-4\nu}\right)+\mathsf{P}_2\sin\left(\frac{1}{2}(\mathsf{k}\varkappa)\sqrt{\mathcal{E}^2-4\nu}\right)\right)}-\frac{\mathcal{E}}{2}\right)^2\Bigg],\\
\mathsf{y}_{\mathsf{t}}(\varkappa,0) &= \vartheta\left(\mathsf{P}_1^2+\mathsf{P}_2^2\right)\sqrt{\mathcal{E}^2-4\nu}\Bigg(\mathsf{P}_1\sin\left(\frac{\varkappa\sqrt{\mathcal{E}^2-4\nu}\sqrt{\mathscr{R}_1+\mathcal{E}\vartheta^2}}{2\sqrt{\mathcal{E}}}\right)\\
&\quad-\mathsf{P}_2\cos\left(\frac{\varkappa\sqrt{\mathcal{E}^2-4\nu}\sqrt{\mathscr{R}_1+\mathcal{E}\vartheta^2}}{2\sqrt{\mathcal{E}}}\right)\Bigg)\Bigg/\Bigg[2\Bigg(\mathsf{P}_1\cos\left(\frac{\varkappa\sqrt{\mathcal{E}^2-4\nu}\sqrt{\mathscr{R}_1+\mathcal{E}\vartheta^2}}{2\sqrt{\mathcal{E}}}\right)\\
&\quad+\mathsf{P}_2\sin\left(\frac{\varkappa\sqrt{\mathcal{E}^2-4\nu}\sqrt{\mathscr{R}_1+\mathcal{E}\vartheta^2}}{2\sqrt{\mathcal{E}}}\right)\Bigg)+\left(\left(\mathsf{P}_1^2-\mathsf{P}_2^2\right)\cos\left(\frac{\varkappa\sqrt{\mathcal{E}^2-4\nu}\sqrt{\mathscr{R}_1+\mathcal{E}\vartheta^2}}{\sqrt{\mathcal{E}}}\right)\right.\\
&\quad\left.+2\mathsf{P}_1\mathsf{P}_2\sin\left(\frac{\varkappa\sqrt{\mathcal{E}^2-4\nu}\sqrt{\mathscr{R}_1+\sigma\vartheta^2}}{\sqrt{\mathcal{E}}}\right)\right)\Bigg],
\end{aligned}
\tag{4.3}
$$

where $\mathscr{R}_0=\frac{\mathscr{R}_1\nu}{\mathcal{E}}$, $\mathscr{R}_2=\frac{\mathscr{R}_1}{\mathcal{E}}$, and $\mathsf{k}=\frac{\sqrt{\mathscr{R}_1+\mathcal{E}\vartheta^2}}{\sqrt{\mathcal{E}}}$.

Using the $CPTM$ and employing the recurrence relation presented in Eq (2.27), we get:

$$
\mathsf{y}_1(\varkappa,\mathsf{t})=\hbar\mathsf{y}_0(\varkappa,\mathsf{t})+(1-\hbar)\mathsf{y}_0-\hbar\mathsf{L}^{-1}\left\{\frac{1}{\mathcal{S}^{\mathfrak{B}}}\mathsf{L}\left[-\mathsf{y}_{0\varkappa\varkappa}+e^{2\mathsf{y}_0}\right]\right\},
\tag{4.4}
$$

where $\mathsf{y}_0=\mathsf{y}(\varkappa,0)+\mathsf{t}\,\mathsf{y}_{\mathsf{t}}(\varkappa,0)$. To find $\mathsf{y}_2,\mathsf{y}_3,...$, we use APs to extract the nonlinear term $e^{2\mathsf{y}}$, where:

$$
\begin{aligned}
&F(\mathsf{y})=e^{2\mathsf{y}},\\
&\mathscr{A}_0=e^{2\mathsf{y}_0},\\
&\mathscr{A}_1=2\mathsf{y}_1e^{2\mathsf{y}_0},\\
&\mathscr{A}_2=2\mathsf{y}_2e^{2\mathsf{y}_0}+\frac{1}{2!}\mathsf{y}_1^2\,4e^{2\mathsf{y}_0}.\\
&\vdots
\end{aligned}
$$

Hence,

$$
\mathsf{y}_2=\hbar\mathsf{y}_0+(1-\hbar)\mathsf{y}_1-\hbar\mathsf{L}^{-1}\left\{\frac{1}{\mathcal{S}^{\mathfrak{B}}}\mathsf{L}\left[-\mathsf{y}_{1\varkappa\varkappa}+2\mathsf{y}_1e^{2\mathsf{y}_0}\right]\right\}.
\tag{4.5}
$$

Using the Mathematica 13.2 software, one can evaluate $\mathsf{y}_1,\mathsf{y}_2,...$; however, due to the extensive computations, we halt at the second term.

Tables 1 and 2 clarify a comparison between the analytical results in reference [22], the approximated results that we obtained, and the absolute error at different values of $\varkappa$ for different time steps. By noticing Figure 3, the region that is parallel to the x-axis is approximately $[-1,0.1]$, and this region includes the values of $\hbar$ in which the solution converges rapidly. Table 1 represents the comparison at $\hbar=-1$ and Table 2 represents the comparison at $\hbar=0.01$. The results we obtained illustrate the efficiency of the $CPTM$ in solving nonlinear $FPDEs$.

Table 1. The analytical results in [22] and the numerical values of $\mathsf{y}(\varkappa,\mathsf{t})$ presented in Eq (4.5), and absolute error at $\mathsf{P}_1 = 0.1, \mathsf{P}_2 = 0.0001, \nu = 0.01, \mathscr{R}_1 = 0.001, \mathcal{E} = 0.001$, and $\vartheta = 0.4$ for $\mathfrak{B} = 2$ at $\hbar = -1$.

	t = 0.01			t = 0.1			t = 0.2		
$\varkappa$	Analy.	Num.	Error	Analy.	Num.	Error	Analy.	Num.	Error
-10	2.05903	2.05903	9.90 E-7	2.05838	2.05828	9.90 E-5	2.05766	2.05726	3.96 E-4
-7	2.13198	2.13198	8.59 E-7	2.13101	2.13093	8.60 E-5	2.12994	2.12960	3.44 E-4
-4	2.22619	2.22619	4.55 E-7	2.22514	2.22510	4.57 E-5	2.22397	2.22379	1.83 E-4
-1	2.29683	2.29683	1.02 E-7	2.29645	2.29646	1.01 E-5	2.29601	2.29605	3.98 E-5
2	2.28067	2.28067	5.01 E-8	2.28136	2.28135	4.80 E-6	2.28212	2.28210	1.83 E-5
5	2.19439	2.19439	6.29 E-7	2.19547	2.19540	6.27 E-5	2.19667	2.19642	2.50 E-4
8	2.10467	2.10467	9.24 E-7	2.10554	2.10545	9.23 E-5	2.10651	2.10614	3.69 E-4

Table 2. The analytical results in [22] and the numerical values of $\mathsf{y}(\varkappa,\mathsf{t})$ presented in Eq (4.5), and absolute error at $\mathsf{P}_1 = 0.1, \mathsf{P}_2 = 0.0001, \nu = 0.01, \mathscr{R}_1 = 0.001, \mathcal{E} = 0.001$, and $\vartheta = 0.4$ for $\mathfrak{B} = 2$ at $\hbar = 0.01$.

	t = 0.01			t = 0.1			t = 0.2		
$\varkappa$	Analy.	Num.	Error	Analy.	Num.	Error	Analy.	Num.	Error
-10	2.05903	2.05903	1.17 E-8	2.05838	2.05838	1.17 E-6	2.05766	2.05766	4.67 E-6
-7	2.13198	2.13198	1.05 E-8	2.13101	2.13101	1.06 E-6	2.12994	2.12994	4.26 E-6
-4	2.22619	2.22619	2.01 E-8	2.22514	2.22514	1.99 E-6	2.22397	2.22398	7.88 E-6
-1	2.29683	2.29683	7.34 E-8	2.29645	2.29645	7.32 E-6	2.29601	2.29604	2.92 E-5
2	2.28067	2.28067	5.83 E-8	2.28136	2.28136	5.85 E-6	2.28212	2.28214	2.35 E-5
5	2.19439	2.19439	5.26 E-9	2.19547	2.19547	5.40 E-7	2.19667	2.19667	2.22 E-6
8	2.10467	2.10467	1.29 E-8	2.10554	2.10554	1.29 E-6	2.10651	2.10651	5.17 E-6

Case II . For $\epsilon = \mathsf{P} = \rho = 2$, $\upsilon = \zeta = 1$, and $\varpi = q^2$.

Using the relation (1.5), the *TF q-deformed TGE* presented in (4.1) transformed into:

$$ {}^{C}\mathfrak{D}_{\mathsf{t}}^{\mathfrak{B}}\mathsf{y}(\varkappa,\mathsf{t}) = \mathsf{y}_{\varkappa\varkappa} - e^{4\mathsf{y}} + 2qe^{2\mathsf{y}}, \qquad 1 < \mathfrak{B} \leq 2, \tag{4.6} $$

subject to:

$$
\begin{aligned}
&\mathsf{y}(\varkappa,0) = \\
&\quad ln\left(\mathscr{R}_0 + \left(\mathscr{R}_1\left(\frac{\sqrt{\mathcal{E}^2-4\nu}\left(\mathsf{P}_2\cos\left(\tfrac{1}{2}\mathsf{k}\varkappa\sqrt{\mathcal{E}^2-4\nu}\right) - \mathsf{P}_1\sin\left(\tfrac{1}{2}\mathsf{k}\varkappa\sqrt{\mathcal{E}^2-4\nu}\right)\right)}{2\left(\mathsf{P}_1\cos\left(\tfrac{1}{2}\mathsf{k}\varkappa\sqrt{\mathcal{E}^2-4\nu}\right) + \mathcal{P}_2\sin\left(\tfrac{1}{2}\mathsf{k}\varkappa\sqrt{\mathcal{E}^2-4\nu}\right)\right)} - \frac{\mathcal{E}}{2}\right)\right)^{0.5}\right), \\
&\mathsf{y}_{\mathsf{t}}(\varkappa,0) = -0.25\sqrt{q}\mathcal{E}\left(\mathsf{P}_1^2+\mathsf{P}_2^2\right)\left(\mathcal{E}^2-4\nu\right)\sqrt{q\nu^2\left(\mathsf{k}^2 - \frac{8q^2}{\mathcal{E}^2-4\nu}\right)}\Bigg/ \\
&\quad \left(\nu\left(0.5\left(\mathsf{P}_1^2+\mathsf{P}_2^2\right)\sqrt{q^2\mathcal{E}^2\left(\mathcal{E}^2-4\nu\right)} + 0.5\left(\mathsf{P}_1^2\sqrt{q^2\mathcal{E}^2\left(\mathcal{E}^2-4\nu\right)} + 2\mathsf{P}_1\mathsf{P}_2 q\mathcal{E}\sqrt{\mathcal{E}^2-4\nu}\right.\right.\right. \\
&\quad \left.\left.\left. -\mathsf{P}_2^2\sqrt{q^2\mathcal{E}^2\left(\mathcal{E}^2-4\nu\right)}\right)\cos\left(\mathsf{k}\varkappa\sqrt{\mathcal{E}^2-4\nu}\right)\right.\right. \\
&\quad \left.\left. - 0.5\left(\mathsf{P}_1^2 q\mathcal{E}\sqrt{\mathcal{E}^2-4\nu} - 2\mathsf{P}_1\mathsf{P}_2\sqrt{q^2\mathcal{E}^2\left(\mathcal{E}^2-4\nu\right)} - \mathsf{P}_2^2 q\mathcal{E}\sqrt{\mathcal{E}^2-4\nu}\right)\sin\left(\mathsf{k}\varkappa\sqrt{\mathcal{E}^2-4\nu}\right)\right)\right),
\end{aligned}
\tag{4.7}
$$

where $\mathscr{R}_0 = \frac{q^2\mathcal{E}^2}{\sqrt{q^2\mathcal{E}^2(\mathcal{E}^2-4\nu)}} + q$, and $\mathscr{R}_1 = \frac{2q^2\mathcal{E}}{\sqrt{q^2\mathcal{E}^2(\mathcal{E}^2-4\nu)}}$.

By substituting into the recurrence relation presented in Eq (2.27), we get:

$$\mathsf{y}_1 = \hbar\mathsf{y}_0 + (1-\hbar)\mathsf{y}_0 - \hbar\mathsf{L}^{-1}\Big\{\frac{1}{\mathcal{S}^{\mathfrak{B}}}\mathsf{L}\Big[-\mathsf{y}_{0\varkappa\varkappa} + e^{4\mathsf{y}_0} - 2qe^{2\mathsf{y}_0}\Big]\Big\}, \tag{4.8}$$

where $\mathsf{y}_0 = \mathsf{y}(\varkappa,0) + \mathsf{t}\ \mathsf{y}_{\mathsf{t}}(\varkappa,0)$. To find the higher iterations $\mathsf{y}_2, \mathsf{y}_3, ...$, we use APs for the nonlinear term $e^{2\mathsf{y}}$ and $e^{4\mathsf{y}}$ where $e^{2\mathsf{y}}$ expanded before in Case I and $e^{4\mathsf{y}}$ expanded as follows:

$$\begin{aligned}
\mathscr{B}_0 &= e^{4\mathsf{y}_0},\\
\mathscr{B}_1 &= 4\,\mathsf{y}_1 e^{4\mathsf{y}_0},\\
&\vdots\\
&\vdots
\end{aligned}$$

hence,

$$\mathsf{y}_2 = \hbar\mathsf{y}_0 + (1-\hbar)\mathsf{y}_1 - \hbar\mathsf{L}^{-1}\Big\{\frac{1}{\mathcal{S}^{\mathfrak{B}}}\mathsf{L}\Big[-\mathsf{y}_{1\varkappa\varkappa} + 4\mathsf{y}_1 e^{4\mathsf{y}_0} - 2q(2\mathsf{y}_1 e^{2\mathsf{y}_0})\Big]\Big\}. \tag{4.9}$$

We can expand other terms, $\mathsf{y}_3, \mathsf{y}_4, ...$ to obtain an approximate solution with high accuracy.

Table 3 shows the values of the analytical solution that was presented in reference [22] and the approximate values we obtained at the same values of all parameters for $\hbar = -0.01$. We chose a value of $\hbar$ equal to -0.01 because, looking at Figure 6, it becomes apparent that the region where the solution converges more rapidly lies on the interval $[-1, 0.1]$. So, any value inside this region gives good accuracy. The results reflect the accuracy of the $CPTM$ as the error is very small.

Table 3. The numerical values of the unknown function $\mathsf{y}(\varkappa,\mathsf{t})$ introduced in Eq (4.9) and the analytical solution obtained in [22], and absolute error at $\mathsf{P}_1 = 0.4$, $\mathsf{P}_2 = 0.01$, $\nu = 0.1$, $\mathsf{k} = 0.3$, $\mathcal{E} = 0.001$, and $q = 0.001$ for $\mathfrak{B} = 2$ for $\hbar = -0.01$.

	t = 0.01			t = 0.1			t = 0.2		
$\varkappa$	Analy.	Num.	Error	Analy.	Num.	Error	Analy.	Num.	Error
-10	3.35615	3.35615	9.55 E-8	3.35689	3.35688	9.57 E-6	3.35773	3.35769	3.83 E-5
-7	3.38502	3.38502	6.85 E-8	3.38600	3.38599	6.82 E-6	3.38708	3.38706	2.72 E-5
-4	3.41786	3.41786	2.72 E-8	3.41877	3.41878	2.81 E-6	3.41978	3.41979	1.16 E-5
-1	3.43986	3.43986	1.42 E-7	3.44015	3.44016	1.43 E-5	3.44044	3.44049	5.74 E-5
2	3.43484	3.43484	1.12 E-7	3.43425	3.43426	1.11 E-5	3.43358	3.43362	4.43 E-5
5	3.40695	3.40695	1.30 E-8	3.40595	3.40595	1.37 E-6	3.40484	3.40484	5.79 E-6
8	3.37435	3.37435	8.36 E-8	3.37345	3.37344	8.37 E-6	3.37245	3.37242	3.34 E-5

To examine the influence of different parameters on the equation, particularly the parameter q, we will resolve the second case, this time considering different initial conditions.

Case II under different initial condition. For the *TF q-deformed TGE* (4.6) constrained by:

$$
\begin{aligned}
&\mathsf{y}(\varkappa,0)=\\
&\quad ln\left(\mathscr{R}_0+\left(\mathscr{R}_1\left(\frac{\sqrt{\mathcal{E}^2-4\nu}\left(\mathsf{P}_1\sinh\left(\frac{1}{2}\mathsf{k}\varkappa\sqrt{\mathcal{E}^2-4\nu}\right)+\mathsf{P}_2\cosh\left(\frac{1}{2}\mathsf{k}\varkappa\sqrt{\mathcal{E}^2-4\nu}\right)\right)}{2\left(\mathsf{P}_1\cosh\left(\frac{1}{2}\mathsf{k}\varkappa\sqrt{\mathcal{E}^2-4\nu}\right)+\mathsf{P}_2\sinh\left(\frac{1}{2}\mathsf{k}\varkappa\sqrt{\mathcal{E}^2-4\nu}\right)\right)}-\frac{\mathcal{E}}{2}\right)\right)^{0.5}\right),\\
&\mathsf{y}_{\mathsf{t}}(\varkappa,0)=-\Bigg(2\sqrt{q}\mathcal{E}\left(\mathsf{P}_1^2\left(\nu-0.25\mathcal{E}^2\right)+\mathsf{P}_2^2\left(0.25\mathcal{E}^2-\nu\right)\right)\sqrt{q\nu^2\left(\mathsf{k}^2-\frac{8q^2}{\mathcal{E}^2-4\nu}\right)}\Bigg)\Big/\\
&\quad\Bigg(\nu\Bigg(-\left(\mathsf{P}_1^2-\mathsf{P}_2^2\right)\sqrt{q^2\mathcal{E}^2\left(\mathcal{E}^2-4\nu\right)}-\Bigg(\mathsf{P}_1^2\sqrt{q^2\mathcal{E}^2\left(\mathcal{E}^2-4\nu\right)}-2\mathsf{P}_1\mathsf{P}_2q\mathcal{E}\sqrt{\mathcal{E}^2-4\nu}\\
&\quad+\mathsf{P}_2^2\sqrt{q^2\mathcal{E}^2\left(\mathcal{E}^2-4\nu\right)}\Bigg)\cosh\left(\mathsf{k}\varkappa\sqrt{\mathcal{E}^2-4\nu}\right)+\left(\mathsf{P}_1^2q\mathcal{E}\sqrt{\mathcal{E}^2-4\nu}\right.\\
&\quad\left.+\mathsf{P}_2^2q\mathcal{E}\sqrt{\mathcal{E}^2-4\nu}-2\mathsf{P}_1\mathsf{P}_2\sqrt{q^2\mathcal{E}^2\left(\mathcal{E}^2-4\nu\right)}\right)\sinh\left(\mathsf{k}\varkappa\sqrt{\mathcal{E}^2-4\nu}\right)\Bigg),
\end{aligned}
\tag{4.10}
$$

where $\mathscr{R}_0=q-\frac{q^2\mathcal{E}^2}{\sqrt{q^2\mathcal{E}^2\left(\mathcal{E}^2-4\nu\right)}}$, and $\mathscr{R}_1=-\frac{2q^2\mathcal{E}}{\sqrt{q^2\mathcal{E}^2\left(\mathcal{E}^2-4\nu\right)}}$.

Using the iterative scheme that we obtained in Eq (2.27) and substituting with the initial conditions to obtain the sequence of solution:

$$
\begin{aligned}
&\mathsf{y}_0=\mathsf{y}(\varkappa,0)+\mathsf{t}\;\mathsf{y}_{\mathsf{t}}(\varkappa,0),\\
&\mathsf{y}_1=\hbar\mathsf{y}_0(\varkappa,\mathsf{t})+(1-\hbar)\mathsf{y}_0-\hbar\mathsf{L}^{-1}\left\{\frac{1}{\mathcal{S}^{\mathfrak{B}}}\mathsf{L}\left[-\mathsf{y}_{0\varkappa\varkappa}+e^{4\mathsf{y}_0}-2qe^{2\mathsf{y}_0}\right]\right\}.\\
&\vdots
\end{aligned}
\tag{4.11}
$$

We can proceed to compute higher terms, but we will halt due to the large and intricate calculations, which constitute the main drawback of this method.

Table 4 shows the analytical results, our obtained results, and the absolute error between the two values under the same values of parameters for $\hbar=-1$. The results are the solution of the *TF q-deformed TGE* for Case II, which is presented in Eq (4.11). The results are at different values of $\varkappa$ and at various values of t.

Table 4. The obtained values for the function $\mathsf{y}(\varkappa,\mathsf{t})$ introduced in Eq (4.11), the analytical solution, and the absolute error at $\mathsf{P}_1=0.3$, $\mathsf{P}_2=0.4$, $\nu=0.001,\mathsf{k}=0.4$, $\mathcal{E}=0.1$, and $q=0.4$ for $\mathfrak{B}=2$ and $\hbar=-1$.

	t = 0.01			t = 0.1			t = 0.2		
$\varkappa$	Analy.	Num.	Error	Analy.	Num.	Error	Analy.	Num.	Error
-10	1.76634	1.76633	9.02 E-6	1.71114	1.71013	1.01 E-3	1.65164	1.64712	4.52 E-3
-7	1.79373	1.79372	8.29 E-6	1.74050	1.73958	9.22 E-4	1.6831	1.67902	4.08 E-3
-4	1.8219	1.82189	7.61 E-6	1.77047	1.76963	8.40 E-4	1.71497	1.71128	3.69 E-3
-1	1.85078	1.85078	6.98 E-6	1.8010	1.80024	7.65 E-4	1.74726	1.74391	3.34 E-3
2	1.88033	1.88033	6.40 E-6	1.83207	1.83137	6.97 E-4	1.77994	1.77691	3.03 E-3
5	1.9105	1.91050	5.87 E-6	1.86364	1.86300	6.36 E-4	1.81300	1.81025	2.75 E-3
8	1.94126	1.94125	5.38 E-6	1.89569	1.89511	5.80 E-4	1.84644	1.84394	2.49 E-3

Table 5 introduces the results that we obtained and the analytical results supported by the absolute error for Case II, which its solution is presented in Eq (4.11), but this time at $\hbar=-0.01$ and $q=0.004$.

Table 5. The obtained values for the function $\mathsf{y}(\varkappa, \mathsf{t})$ introduced in Eq (4.11), the analytical solution, and the absolute error at $\mathsf{P}_1 = 0.3$, $\mathsf{P}_2 = 0.4$, $\nu = 0.001, \mathsf{k} = 0.4$, $\mathcal{E} = 0.1$, and $q = 0.004$ for $\mathfrak{B} = 2$ and $\hbar = -0.01$.

	t = 0.01			t = 0.1			t = 0.2		
$\varkappa$	Analy.	Num.	Error	Analy.	Num.	Error	Analy.	Num.	Error
-10	3.49675	3.49675	3.02 E-9	3.49819	3.49819	3.22 E-7	3.49979	3.49978	1.36 E-6
-7	3.54785	3.54785	2.64 E-9	3.54926	3.54926	2.81 E-7	3.55083	3.55083	1.18 E-6
-4	3.59811	3.59811	2.33 E-9	3.59950	3.59950	2.47 E-7	3.60105	3.60104	1.03 E-6
-1	3.64763	3.64763	2.05 E-9	3.64901	3.64901	2.17 E-7	3.65053	3.65053	9.14 E-7
2	3.69652	3.69652	1.82 E-9	3.69788	3.69788	1.92 E-7	3.69938	3.69938	8.07 E-7
5	3.74484	3.74484	1.62 E-9	3.74619	3.74619	1.70 E-7	3.74768	3.74768	7.15 E-7
8	3.79268	3.79268	1.44 E-9	3.79401	3.79401	1.52 E-7	3.79549	3.79548	6.35 E-7

5. Visual representations

Graphical depictions, whether in 2D or 3D, provide an innovative way to showcase the behavior of the model under study. These graphics allow for a direct comparison between the precise and approximate solutions and also clarify the relations between all parameters that affect the equation. In this investigation, we address the *TF q-deformed TGE* according to different initial conditions. Figure 1 presents the two-dimensional depiction of the solution obtained from the proposed model, incorporating starting conditions specified in Case I. In Figure 1(a), the depiction varies at varying the fractional order parameter values $\mathfrak{B}$ with a constant time of $\mathsf{t} = 3$. In Figure 1(b), the illustration remains constant at $\mathfrak{B} = 2$ but varies across different time intervals. Figure 2 depicts the three-dimensional setup of Case I, where Figure 2(a) elucidates the approximate solution derived in this study, while Figure 2(b) showcases the analytical solution outlined in [22]. The graphs exhibit a high degree of consistency under identical conditions, indicating the accuracy of the solutions obtained. Figures 4 and 5 represent the 2D and 3D approximate solution we obtained for the second case at convergence parameter $\hbar = -0.01$. We choose the value of $\hbar$ such that it is located in the interval that parallel to x-axis as presented in Figures 3 and 6. Figure 7 shows the effect of the deformation parameter q on the shape of the wave solution using initial conditions in Case I at fixed time $\mathsf{t} = 1$, $\mathfrak{B} = 2$, and $\hbar = -0.01$. Figure 7(a) presents small values of q; in this case, decreasing q tends to dampen nonlinear effects in the equation, which can lead to smoother and more regular behavior in the solution, with less pronounced solitons and nonlinear waves. While increasing the values of q as presented in Figure 7(b) leads to stronger nonlinear effects in the equation, this can result in the amplification of soliton-like structures and nonlinear waves in the system. Figures 8 and 9 depict the solution of the *TF q-deformed TGE* (Case II) under varying initial conditions specified in Eq (4.10), elucidating the influence of initial parameters on solution behavior for deformation parameter $q = 0.4$. Figure 10 presents the solution of the *TF q-deformed TGE* (Case II) at $q = 0.004$. Figure 11 presents the solution of the *TF q-deformed TGE* with initial conditions specified in Eq (4.10) at fixed $\mathfrak{B} = 2$ and $\hbar = -0.01$ at different values of q.

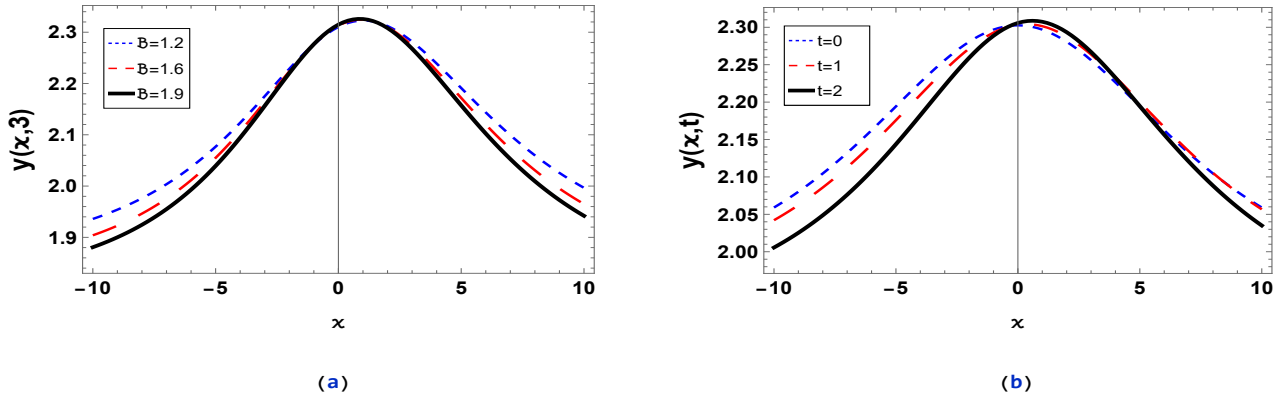

(a) (b)

Figure 1. The calculated solution of *TF q-deformed TGE* (Case I) shown in Eq (4.5) using *CPTM* at $\mathsf{P}_1 = 0.1, \mathsf{P}_2 = 0.0001, \nu = 0.01, \mathscr{R}_1 = 0.001, \mathcal{E} = 0.001$ and $\vartheta = 0.4$ for $\hbar = -1$. (a) At t = 3 for various values of $\mathfrak{B}$. (b) At $\mathfrak{B} = 2$ for several steps of time.

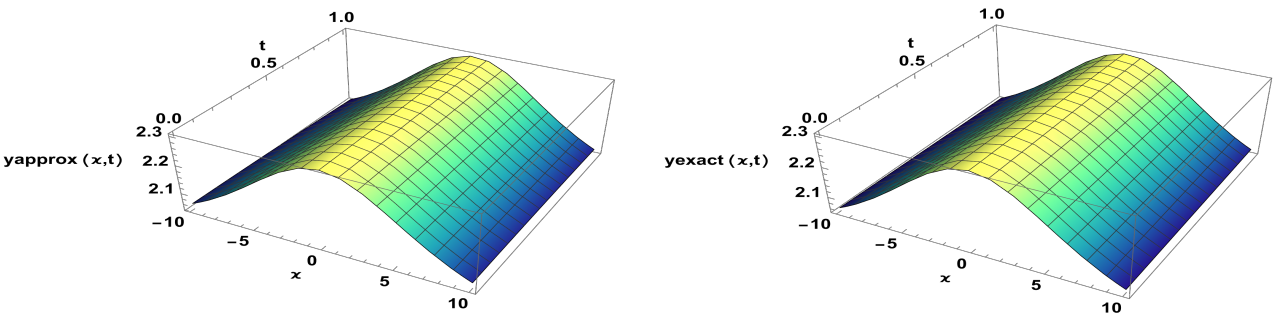

(a) (b)

Figure 2. The three-dimensional representation of the *TF q-deformed TGE* (Case I) at $\mathsf{P}_1 = 0.1, \mathsf{P}_2 = 0.0001, \nu = 0.01, \mathscr{R}_1 = 0.001, \mathcal{E} = 0.001$, $\vartheta = 0.4$, and $\mathfrak{B} = 2$. (a) The estimated solution presented in Eq (4.5) at $\hbar = -1$. (b) The exact solution.

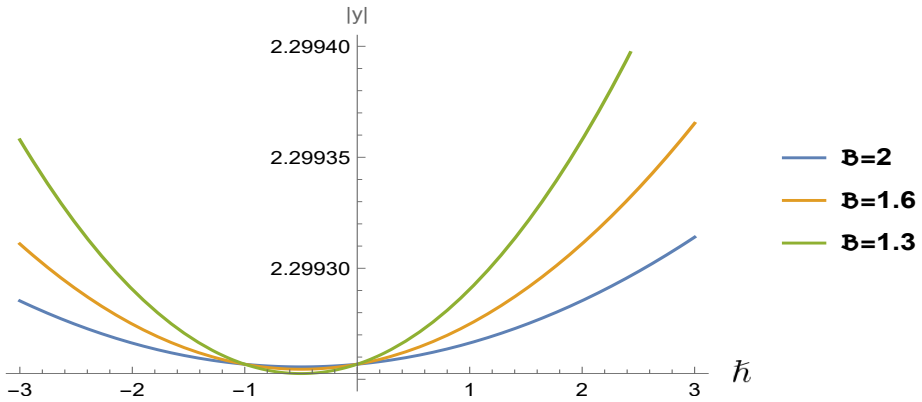

Figure 3. The graphs of the $\hbar$-curves of the *TF q-deformed TGE* (Case I) at $\mathsf{P}_1 = 0.1, \mathsf{P}_2 = 0.0001, \nu = 0.01, \mathscr{R}_1 = 0.001, \mathcal{E} = 0.001$, and $\vartheta = 0.4$ at $\varkappa = 0.8$ and t = 0.1 at various values of $\mathfrak{B}$.

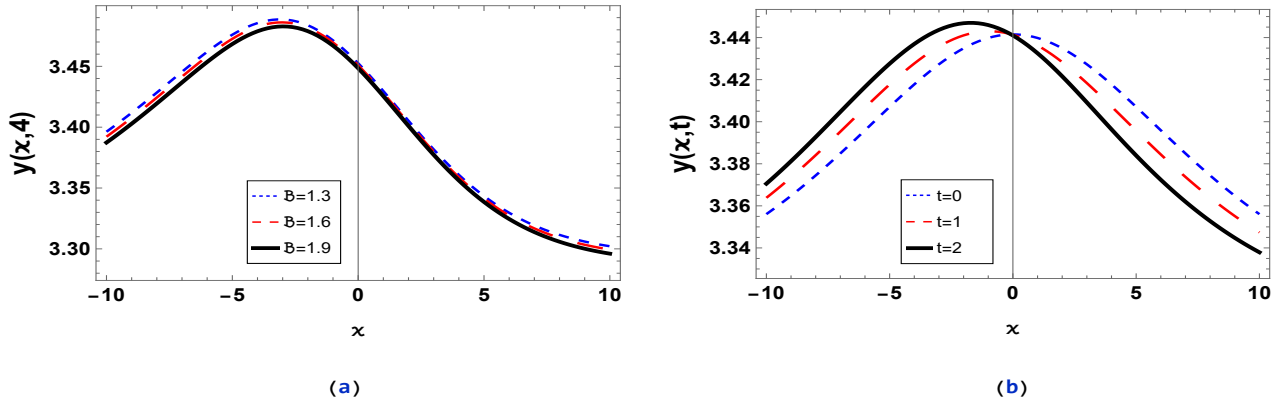

Figure 4. The calculated solution of *TF q-deformed TGE* (Case II) shown in (4.9) using *CPTM* at $\mathsf{P}_1 = 0.4$, $\mathsf{P}_2 = 0.01$, $\nu = 0.1$, $\mathsf{k} = 0.3$, $\mathcal{E} = 0.001$, and $q = 0.001$ for $\hbar = -0.01$. (a) At $\mathsf{t} = 4$ for various values of $\mathfrak{B}$. (b) At $\mathfrak{B} = 2$ for several steps of time.

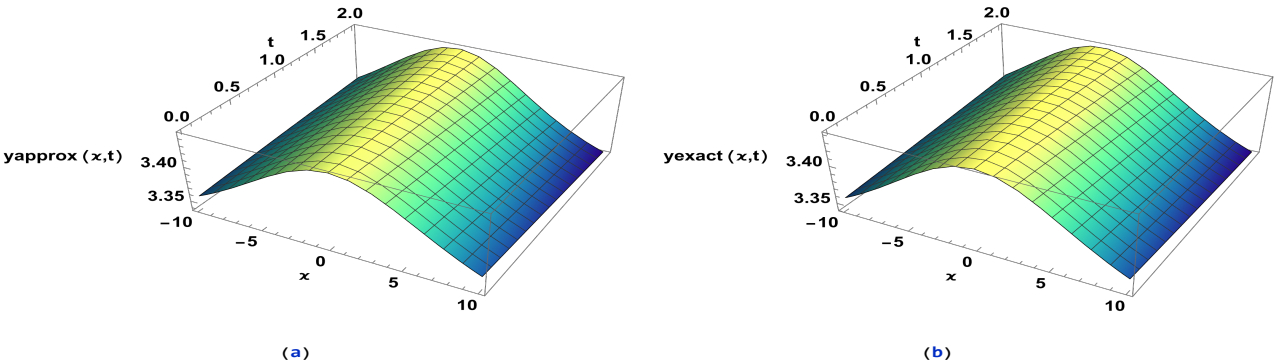

Figure 5. The 3D representation of the solution of *TF q-deformed TGE* (Case II) at $\mathsf{P}_1 = 0.4$, $\mathsf{P}_2 = 0.01$, $\nu = 0.1$, $\mathsf{k} = 0.3$, $\mathcal{E} = 0.001$, $q = 0.001$ and $\mathfrak{B} = 2$ for $\hbar = -0.01$. (a) The estimated solution presented in (4.9). (b) The exact solution.

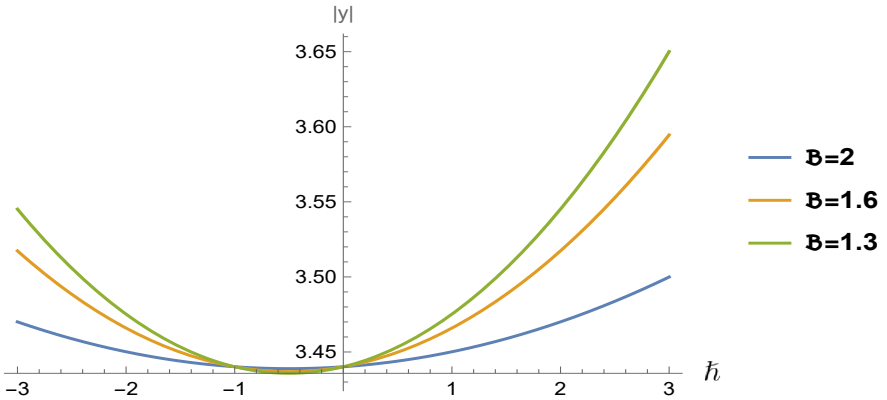

Figure 6. The $\hbar$-curves of the *TF q-deformed TGE* (Case II) at $\mathsf{P}_1 = 0.4$, $\mathsf{P}_2 = 0.01$, $\nu = 0.1$, $\mathsf{k} = 0.3$, $\mathcal{E} = 0.001$, and $q = 0.001$ at $\varkappa = 0.8$ and $\mathsf{t} = 0.1$ for different values of $\mathfrak{B}$.

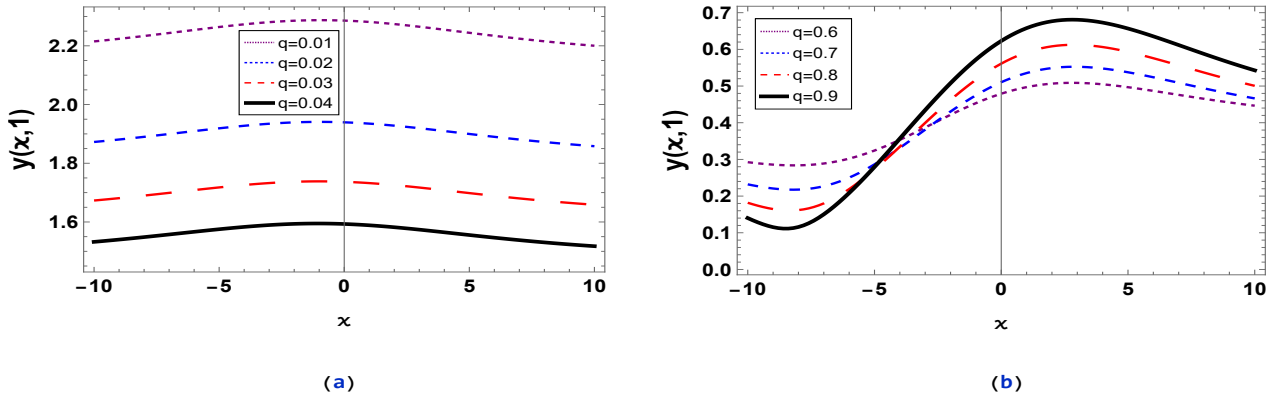

Figure 7. The approximate solution of *TF q-deformed TGE* (Case II) presented in (4.9) at $\mathsf{P}_1 = 0.4$, $\mathsf{P}_2 = 0.01$, $\nu = 0.1$, $\mathsf{k} = 0.3$, $\mathcal{E} = 0.001$, $\mathsf{t} = 1$, and $\mathfrak{B} = 2$ at various q values for $\hbar = -0.01$.

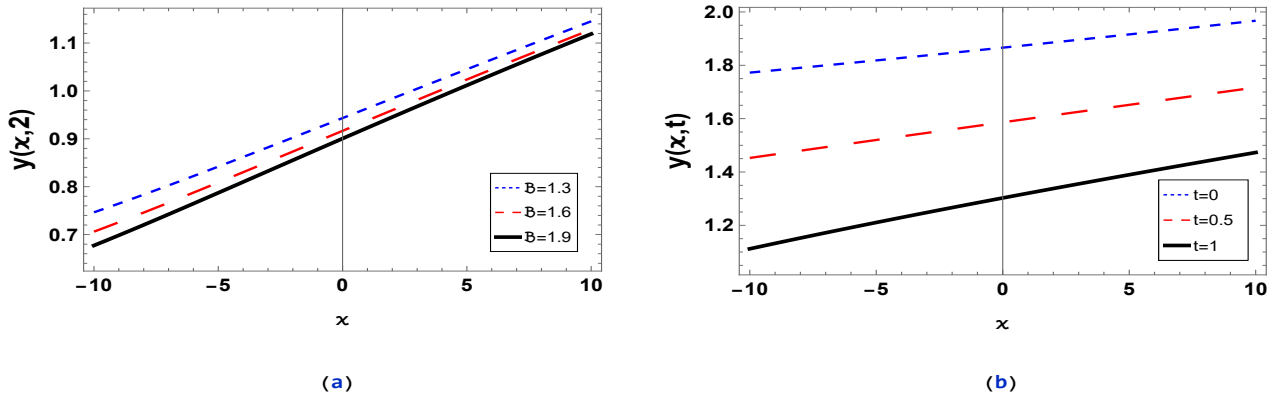

Figure 8. The calculated solution of *TF q-deformed TGE* (Case II) presented in (4.11) at $\mathsf{P}_1 = 0.3$, $\mathsf{P}_2 = 0.4$, $\nu = 0.001$, $\mathsf{k} = 0.4$, $\mathcal{E} = 0.1$, and $q = 0.4$ for $\hbar = -1$. (a) At $\mathsf{t} = 2$ for various values of $\mathfrak{B}$ (b) At $\mathfrak{B} = 2$ for distinct values of t.

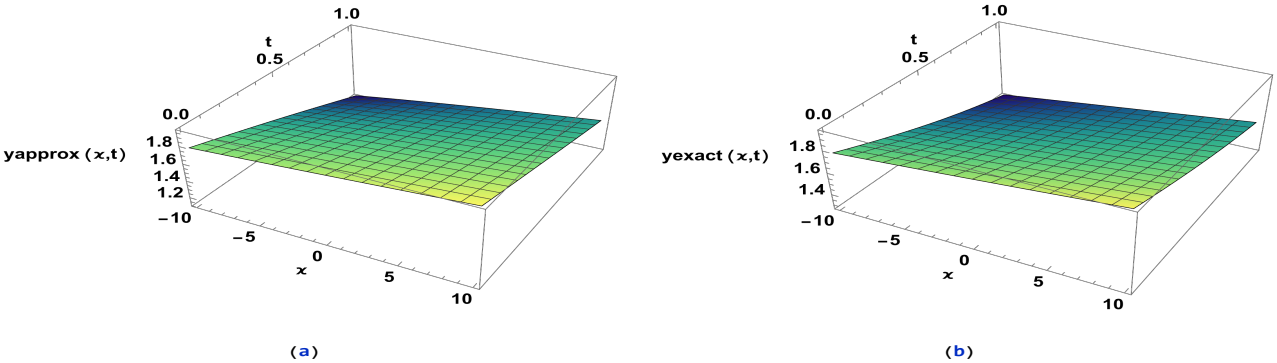

Figure 9. The 3D representation of the solution of *TF q-deformed TGE* (Case II) presented in (4.11) at $\mathsf{P}_1 = 0.3$, $\mathsf{P}_2 = 0.4$, $\nu = 0.001$, $\mathsf{k} = 0.4$, $\mathcal{E} = 0.1$, $q = 0.4$ and $\mathfrak{B} = 2$. (a) The estimated solution when $\hbar = -1$. (b) The exact solution.

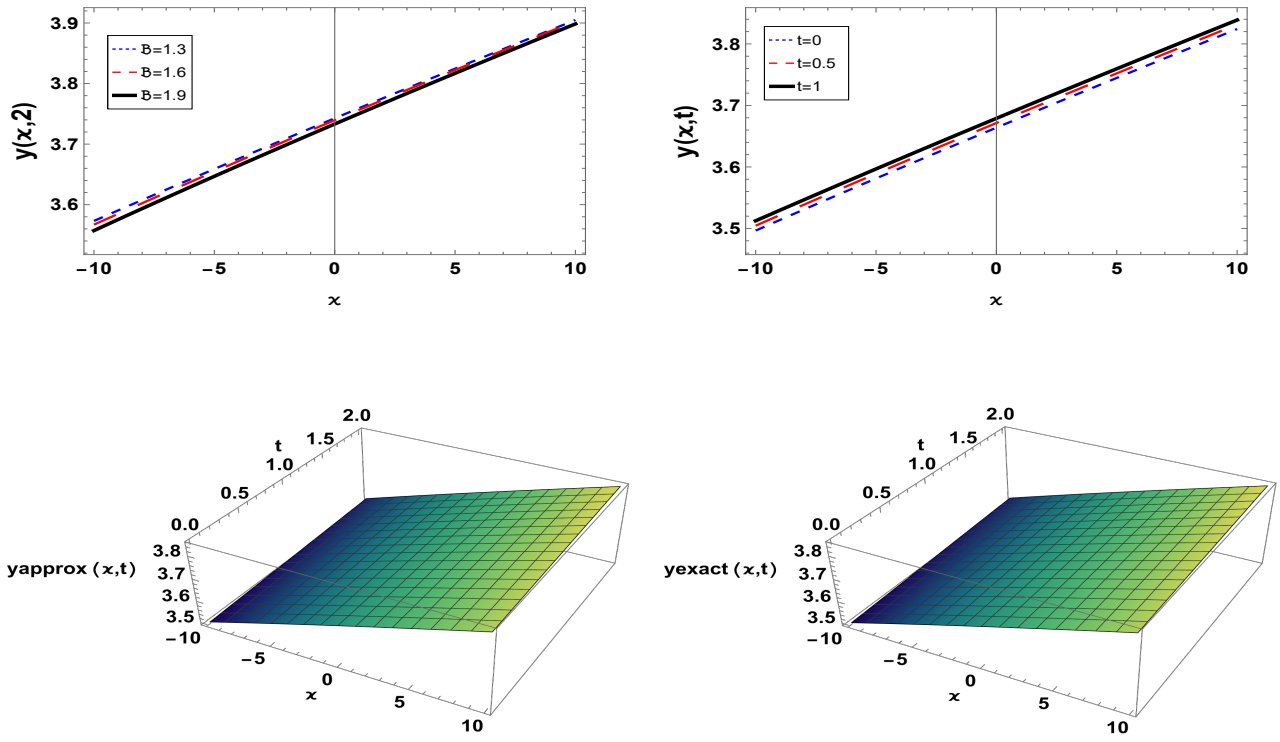

Figure 10. 2D and 3D representation of the solution of *TF q-deformed TGE* (Case II) presented in (4.11) at $\mathsf{P}_1 = 0.3$, $\mathsf{P}_2 = 0.4$, $\nu = 0.001$, $\mathsf{k} = 0.4$, $\mathcal{E} = 0.1$, $q = 0.004$ and $\mathfrak{B} = 2$ for $\hbar = -0.01$.

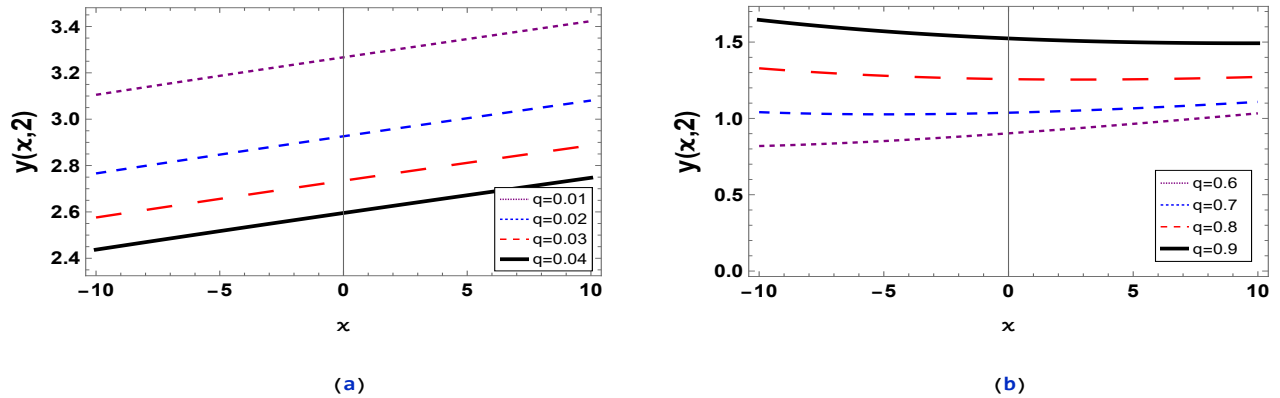

Figure 11. The calculated solution of *TF q-deformed TGE* (Case II) presented in (4.11) at $\mathsf{P}_1 = 0.3$, $\mathsf{P}_2 = 0.4$, $\nu = 0.001$, $\mathsf{k} = 0.4$, $\mathcal{E} = 0.1$, $\mathsf{t} = 2$, and $\mathfrak{B} = 2$ at various values of q for $\hbar = -0.01$.

6. Conclusions

This paper has introduced a revolutionary equation, the *TF q-deformed TGE*, representing a significant breakthrough in mathematical physics. This innovative equation combines fractional

calculus and q-deformation, providing a flexible framework for modeling physical systems with violated symmetries. The novelty of our approach lies in solving this equation in fractional form utilizing the $CPTM$, known for its effectiveness in handling such equations. Our results demonstrate the efficiency and accuracy of this method, as evident from the absolute error calculations presented in the corresponding tables for each case. We have investigated both the existence and the uniqueness of the solution. Additionally, the depiction of various 2D and 3D graphs has provided insights into the impact of different parameters on the solution's behavior.

For the future directions in exploring the TF *q-deformed* TGE, we aim to investigate this equation with boundary conditions and incorporate additional elements such as external source term. Furthermore, examining the stability and numerical implementation of this equation could facilitate practical applications and simulations across a range of domains.

Authors Contributions

All authors of this article have been contributed equally. All authors have read and approved the final version of the manuscript for publication.

Use of AI tools declaration

The authors declare they have not used Artificial Intelligence (AI) tools in the creation of this article in any part at all.

Acknowledgment

The authors extend their appreciation to Taif University, Saudi Arabia, for supporting this work through project number (TU-DSPP-2024-73).

Conflict of interest

There is no conflict of interest between the authors or anyone else regarding this manuscript.

References

1. A. A. Kilbas, H. M. Srivastava, J. J. Trujillo, *Theory and applications of fractional differential equations*, Amsterdam: Elsevier, 2006.
2. M. P. Lazarevic, *Advanced topics on applications of fractional calculus on control problems, system stability and modeling*, WSEAS Press, 2014.
3. S. S. Ray, *Nonlinear differential equations in physics*, Springer Singapore, 2020. https://doi.org/10.1007/978-981-15-1656-6
4. A. Elsaid, M. S. A. Latif, M. Maneea, Similarity solutions for multiterm time-fractional diffusion equation, *Adv. Math. Phys.*, **2016** (2016), 7304659. http://dx.doi.org/10.1155/2016/7304659

5. M. S. A. Latif, D. Baleanu, A. H. A. Kader, Exact solutions for a class of variable coefcients fractional diferential equations using Mellin transform and the invariant subspace method, *Differ. Equ. Dyn. Syst.*, 2024. https://doi.org/10.1007/s12591-024-00680-3

6. P. Kulczycki, J. Korbicz, J. Kacprzyk, *Fractional dynamical systems: Methods, algorithms and applications*, **402** (2022), Switzerland: Springer. https://doi.org/10.1007/978-3-030-89972-1

7. K. K. Ali, M. Maneea, M. S. Mohamed, Solving nonlinear fractional models in superconductivity using the q-Homotopy analysis transform method, *J. Math.*, **2023** (2023), 6647375. https://doi.org/10.1155/2023/6647375

8. T. A. Sulaiman, H. Bulut, H. M. Baskonus, Optical solitons to the fractional perturbed NLSE in nano-fibers, *Discrete Cont. Dyn. S.*, **13** (2020), 925–936. http://dx.doi.org/10.3934/dcdss.2020054

9. K. Engelborghs, V. Lemaire, J. Belair, D. Roose, Numerical bifurcation analysis of delay differential equations arising from physiological modeling, *J. Math. Biol.*, **42** (2001), 361–385. https://doi.org/10.1007/s002850000072

10. J. F. Gómez, L. Torres, R. F. Escobar, *Fractional derivatives with Mittag-Leffler kernel*, Switzerland: Springer International Publishing, **194** (2019). https://doi.org/10.1007/978-3-030-11662-0

11. Z. Y. Fan, K. K. Ali, M. Maneea, M. Inc, S. W. Yao, Solution of time fractional Fitzhugh-Nagumo equation using semi analytical techniques, *Results Phys.*, **51** (2023), 106679. https://doi.org/10.1016/j.rinp.2023.106679

12. O. G. Gaxiola, S. O. Edeki, O. O. Ugbebor, J. Ruiz de Chavez, Solving the Ivancevic pricing model using the He's frequency amplitude formulation, *Eur. J. Pure Appl. Math.*, **10** (2017), 631–637.

13. K. K. Ali, M. A. Maaty, M. Maneea, Optimizing option pricing: Exact and approximate solutions for the time-fractional Ivancevic model, *Alex. Eng. J.*, **84** (2023), 59–70. https://doi.org/10.1016/j.aej.2023.10.066

14. A. Arai, Exactly solvable supersymmetric quantum mechanics, *J. Math. Anal. Appl.*, **158** (1991), 63–79. https://doi.org/10.1016/0022-247X(91)90267-4

15. U. Carow-Watamura, S. Watamura, The q-deformed Schrodinger equation of the harmonic oscillator on the quantum Euclidean space, *Int. J. Mod. Phys. A.*, **9** (1994), 3898–4008. https://doi.org/10.1142/S0217751X94001618

16. A. Dobrogowska, A. Odzijewicz, Solutions of the q-deformed Schrödinger equation for special potentials, *J. Phys. A: Math. Theor.*, **40** (2023). https://doi.org/10.1088/1751-8113/40/9/008

17. B. C. Lutfuoglu, A. N. Ikot, E. O. Chukwocha, F. E. Bazuaye, Analytical solution of the Klein Gordon equation with a multi-parameter q-deformed Woods-Saxon type potential, *Eur. Phys. J. Plus*, **133** (2018). https://doi.org/10.1140/epjp/i2018-12299-y

18. H. Eleuch, Some analytical solitary wave solutions for the generalized q-deformed Sinh-Gordon equation: $\frac{\partial^2 u}{\partial z \partial \zeta} = e^{\Theta u}[sinh_q(u^\gamma)]^p - \delta$, *Adv. Math. Phys.*, **2018** (2018), 5242757. https://doi.org/10.1155/2018/5242757

19. H. I. Alrebdi, N. Raza, S. Arshed, A. R. Butt, A. Abdel-Aty, C. Cesarano, et al., A variety of new explicit analytical soliton solutions of q-deformed Sinh-Gordon in (2+1) dimensions, *Symmetry*, **14** (2022), 2425. https://doi.org/10.3390/sym14112425

20. N. Raza, S. Arshed, H. I. Alrebdi, A. Abdel-Aty, H. Eleuch, Abundant new optical soliton solutions related to q-deformed Sinh-Gordon model using two innovative integration architectures, *Results Phys.*, **35** (2022), 105358. https://doi.org/10.1016/j.rinp.2022.105358

21. K. K. Ali, M. S. Mohamed, M. Maneea, Exploring optical soliton solutions of the time fractional q-deformed Sinh-Gordon equation using a semi-analytic method, *AIMS Math.*, **8** (2023), 27947–27968. https://doi.org/10.3934/math.20231429

22. K. K. Ali, W. G. Alharbi, Exploring unconventional optical soliton solutions for a novel q-deformed mathematical model, *AIMS Math.*, **9** (2024), 15202–15222. https://doi.org/10.3934/math.2024738

23. A. F. Fareed, M. A. Elsisy, M. S. Semary, M. T. M. M. Elbarawy, Controlled Picard's transform technique for solving a type of time fractional Navier-Stokes equation resulting from incompressible fluid flow, *Int. J. Appl. Comput. Math.*, **8** (2022). https://doi.org/10.1007/s40819-022-01361-x

24. S. G. Samko, A. A. Kilbas, O. L. Marichev, *Fractional integrals and derivatives: Theory and applications*, New York: Gordon and Breach, 1993. https://api.semanticscholar.org/CorpusID:118631078

25. I. Podlubny, *Fractional differential equations*, San Diego: Academic Press, 1999.

26. M. Caputo, M. Fabrizio, A new definition of fractional derivative without singular kernel, *Progr. Fract. Differ. Appl.*, **1** (2015), 73–85.

27. A. Elsaid, M. S. A. Latif, M. Maneea, Similarity solutions for solving Riesz fractional partial differential equations, *Progr. Fract. Differ. Appl.*, **2** (2016), 293–298. http://dx.doi.org/10.18576/pfda/020407

28. G. Adomian, R. Rach, Modified Adomian polynomials, *Math. Comput. Model.*, **24** (1996), 39–46. https://doi.org/10.1016/S0895-7177(96)00171-9

29. H. Fatoorehchi, H. Abolghasemi, Improving the differential transform method: A novel technique to obtain the differential transforms of nonlinearities by the Adomian polynomials, *Appl. Math. Model.*, **37** (2013), 6008–6017. https://doi.org/10.1016/j.apm.2012.12.007

30. G. C. Wu, D. Baleanu, W. H. Luo, Analysis of fractional nonlinear diffusion behaviors based on Adomian polynomials, *Therm. Sci.*, **21** (2017), 813–817. https://doi.org/10.2298/TSCI160416301W

31. M. Turkyilmazoglu, Accelerating the convergence of Adomian decomposition method (ADM), *J. Comput. Sci.*, **31** (2019), 54–59. https://doi.org/10.1016/j.jocs.2018.12.014

32. A. M. S. Mahdy, A. Mtawa, Numerical study for the fractional optimal control problem using Sumudu transform method and Picard method, *Mitt. Klosterneuburg*, **66** (2016), 41–59.

33. M. S. Semary, H. N. Hassan, A. G. Radwan, Controlled Picard method for solving nonlinear fractional reaction-diffusion models in porous catalysts, *Chem. Eng. Commun.*, **204** (2017), 635–647. https://doi.org/10.1080/00986445.2017.1300151

34. R. S. Palais, A simple proof of the Banach contraction principle, *J. Fixed Point Theory Appl.*, **2** (2007), 221–223. https://doi.org/10.1007/s11784-007-0041-6

35. J. Garcia-Falset, K. Latrach, E. Moreno-Gàlvez, M. A. Taoudi, Schaefer-Krasnoselskii fixed point theorems using a usual measure of weak noncompactness, *J. Differ. Equ.*, **252** (2012), 3436–3452. https://doi.org/10.1016/j.jde.2011.11.012

AIMS Press

© 2024 the Author(s), licensee AIMS Press. This is an open access article distributed under the terms of the Creative Commons Attribution License (http://creativecommons.org/licenses/by/4.0)